

# Accepted Manuscript

Design, synthesis and biological evaluation of novel pyrenyl derivatives as anticancer agents

Debasish Bandyopadhyay, Jorge L. Sanchez, Adrian M. Guerrero, Fang-Mei Chang, Jose C. Granados, John D. Short, Bimal K. Banik



PII: S0223-5234(14)00891-5

DOI: [10.1016/j.ejmech.2014.09.072](https://doi.org/10.1016/j.ejmech.2014.09.072)

Reference: EJMECH 7379

To appear in: *European Journal of Medicinal Chemistry*

Received Date: 19 July 2014

Revised Date: 19 September 2014

Accepted Date: 23 September 2014

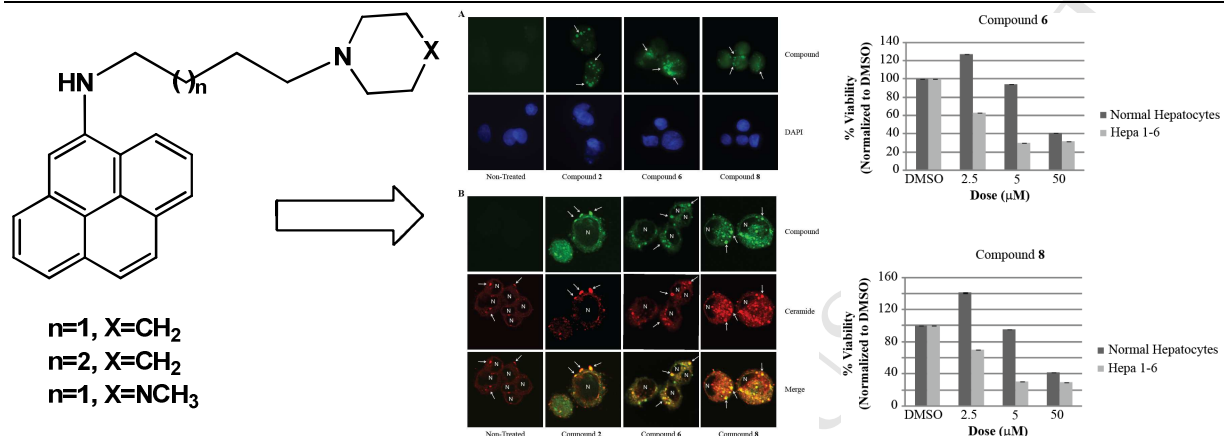
Please cite this article as: D. Bandyopadhyay, J.L. Sanchez, A.M. Guerrero, F.-M. Chang, J.C. Granados, J.D. Short, B.K. Banik, Design, synthesis and biological evaluation of novel pyrenyl derivatives as anticancer agents, *European Journal of Medicinal Chemistry* (2014), doi: 10.1016/j.ejmech.2014.09.072.

This is a PDF file of an unedited manuscript that has been accepted for publication. As a service to our customers we are providing this early version of the manuscript. The manuscript will undergo copyediting, typesetting, and review of the resulting proof before it is published in its final form. Please note that during the production process errors may be discovered which could affect the content, and all legal disclaimers that apply to the journal pertain.

## Graphical abstract

## Design, synthesis and biological evaluation of novel pyrenyl derivatives as anticancer agents

Debasish Bandyopadhyay, Jorge L. Sanchez, Adrian M. Guerrero, Fang-Mei Chang, Jose C. Granados, John D. Short, and Bimal K. Banik



## Design, synthesis and biological evaluation of novel pyrenyl derivatives as anticancer agents

Debashish Bandyopadhyay<sup>1</sup>, Jorge L. Sanchez<sup>1,2</sup>, Adrian M. Guerrero<sup>1</sup>, Fang-Mei Chang<sup>2</sup>, Jose C. Granados<sup>2</sup>, John D. Short<sup>2,3,\*</sup>, and Bimal K. Banik<sup>1,\*</sup>

<sup>1</sup>Department of Chemistry, The University of Texas-Pan American, 1201 West University Drive, Edinburg, Texas 78539, USA

<sup>2</sup>University of Texas Health Science Center at San Antonio-Regional Academic Health Center, Medical Research Division, 1214 West Schunior Street, Edinburg, TX 78541, USA

<sup>3</sup>Department of Pharmacology, University of Texas Health Science Center at San Antonio, 7703 Floyd Curl Drive, San Antonio, TX 78229, USA

\*Corresponding authors, Ph: +1(956)6658741, Fax: +1(956)3845006, E-mails: [banik@utpa.edu](mailto:banik@utpa.edu) or [shortj@uthscsa.edu](mailto:shortj@uthscsa.edu)

### ABSTRACT

Polycyclic aromatic hydrocarbons are widespread in nature with a toxicity range from non-toxic to extremely toxic. A series of pyrenyl derivatives has been synthesized following a four-step strategy where the pyrene nucleus is attached with a basic heterocyclic moiety through a carbon linker. Virtual screening of the physicochemical properties and druggability have been carried out. The cytotoxicity of the compounds (**1–8**) have been evaluated *in vitro* against a small panel of human cancer cell lines which includes two liver cancer (HepG2 and Hepa 1–6), two colon cancer (HT–29 and Caco–2) and one each for cervical (HeLa) and breast (MCF-7) cancer cell lines. The IC<sub>50</sub> data indicate that compound **6** and **8** are the most effective cytotoxic agents in the present set of pyrenyl derivatives, suggesting that having a 4-carbon linker is more effective than a 5-carbon linker and the presence of amide carbonyl groups in the linker severely reduces the efficacy of the compound. The compounds showed selectivity toward cancer cells at lower doses (< 5  $\mu$ M) when compared with the normal hepatocytes. The mechanism of action

supports the cell death through apoptosis in a caspase-independent manner without cleavage of poly (ADP-ribose) polymerase (PARP), even though the compounds cause plasma membrane morphological changes. The compounds, whether highly cytotoxic or mildly cytotoxic, localize to the membrane of cells. The compounds with either a piperidine ring (**6**) or an *N*-methyl piperazine (**8**) in the side chain were both capable of circumventing the drug resistance in SKOV3-MDR1-M6/6 ovarian cancer cells overexpressing P-glycoprotein. Qualitative structure-activity relationship has also been studied.

**KEYWORDS**

Polycyclic, PAH, Pyrene, Anticancer, Cytotoxicity, Apoptosis, Drug resistance.

## 1. Introduction

According to NASA's announcement on February 21, 2014, more than 20% percent of the carbon in the universe is confined in polycyclic aromatic hydrocarbons (PAHs) [1], some of which are considered potent atmospheric pollutants [2]. These PAHs are widely distributed in nature. For example, significant amounts of PAHs are found in natural crude oil and coal deposits, and they are also found in processed fossil fuels, tar and various edible oils [3]. Nevertheless, some PAHs have been identified as carcinogenic, mutagenic or teratogenic [4]. PAHs are soluble in lipid, can be metabolized by cytochrome P450 enzymes, and can interact with cellular components like protein and nucleic acid. Because of this metabolic activation of PAHs, they are considered as indirect acting carcinogens [5]. The toxicity of polycyclic aromatic hydrocarbons (PAHs) is structure-dependent. For example, different PAHs with the same formula and number of rings can vary from being nontoxic to extremely toxic [6]. A key factor in PAH toxicity is the formation of reactive metabolites, and not all PAHs are of the same toxicity because of differences in structure that affect metabolism.

Alternatively, certain PAHs have been identified as antitumoral. For example, the antitumoral anthracyclines (daunorubicin and doxorubicin) and the synthetic anthracene-9,10-dione (mitoxantrone) are potent agents in clinical use today with broad application in the treatment of several leukemias, lymphomas and solid tumors, as well as in combination chemotherapy of solid tumors [7,8]. Additionally, some PAHs have been identified as DNA intercalating agents, an important class of antitumoral DNA binders that are characterized by the insertion of their planar aromatic or heteroaromatic rings between DNA base pairs. For example, anthracyclines, acridines, and ellipticines are DNA intercalating agents [9,10] that are thought to poison topoisomerases I and II [11].

Cancer is a leading cause of death worldwide and accounted for 8.2 million deaths in 2012 among which 70% occur in low- and middle-income countries. According to the World Health Organization the annual cancer cases will rise from 14 million in 2012 to 22 within the next two decades [12,13]. Therefore, a better understanding of how PAHs induce or inhibit carcinogenesis could lower tumor incidence or help fight this disease. Cancer cells often adapt to develop resistance to chemotherapeutic agents, in part through increased expression of protein efflux pumps, which translocate drugs out of the cell [14]. Therefore, it is also important to develop

novel chemotherapeutic agents, including PAHs, which are more potent tumor-selective cytotoxic agents and can circumvent drug resistant cancer cells.

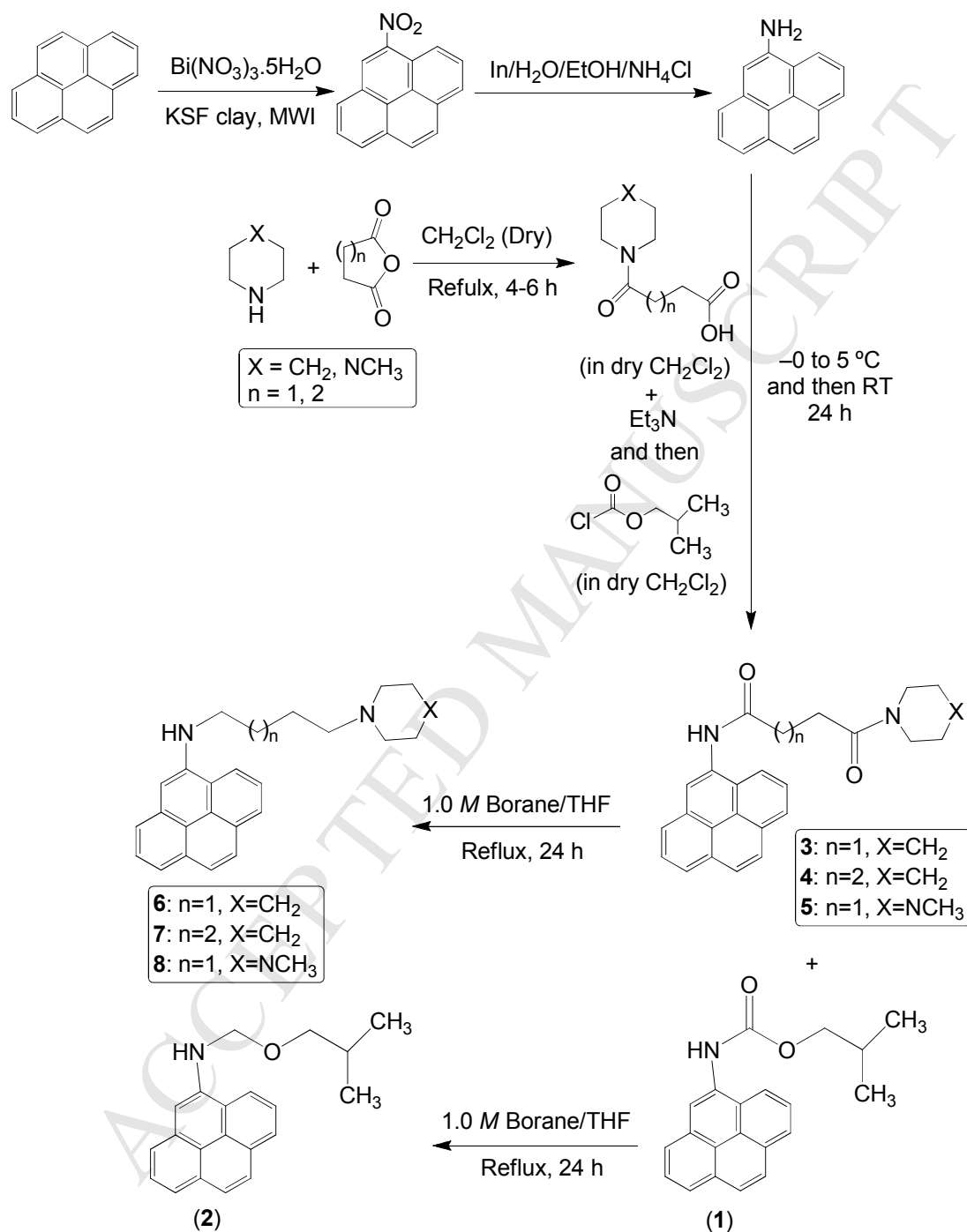
We reported the novel synthesis of chrysenyl or pyrenyl compounds coupled to side chains using bismuth nitrate pentahydrate and microwave irradiation [15], an emerging field of research in synthetic organic chemistry. In fact, we have demonstrated the synthetic uses of trivalent bismuth nitrate pentahydrate in a number of examples, resulting in various methods which includes but are not limited to, nitration of aromatic systems [16,17], Paal-Knorr synthesis of pyrroles [18–21], electrophilic substitution of indoles [22], synthesis of  $\alpha$ -aminophosphonates [23], Hantzsch synthesis of 1,4-dihydropyridines [24], anticancer quinoxalines [25], bioactive benzimidazoles [26] etc. Microwave-induced synthesis of bioactive molecules has also been reported from our laboratory [27–30]. The previous reported pyrenyl compounds exhibited autofluorescent properties and were moderately cytotoxic against selected cancer cell lines (Table 3; Compound **1** and ref 15). However, the cellular and molecular effect(s) of these molecules was not examined in our previous study. Herein, we have used organo-bismuth chemistry to synthesize even more effective anticancer pyrenyl-coupled compounds, and we have examined the molecular and cellular mechanisms by which these compounds cause cytotoxicity. Importantly, we have shown these novel pyrenyl compounds to selectively target cancer cell lines and are capable of circumventing MDR-1-mediated drug resistance in cancer cells. A few analogous compounds derived from chrysene were reported previously [31–33]. The rationale of synthesizing the pyrenyl derivatives reported in this paper is to introduce more effective (against cancer cells) and less toxic (against normal cells) anticancer agents following the U.S. Environmental Protection Agency (EPA) guidelines of polycyclic aromatic hydrocarbons, since chrysene belongs to the list of “probable human carcinogens” while pyrene belongs to “not classifiable as to human carcinogenicity” list [34].

## 2. Results and Discussion

### 2.1. Chemistry

The first step of the present synthesis involves bismuth nitrate induced nitration of pyrene under microwave irradiation. The product 1-nitropyrene was successfully reduced to the corresponding amine with excellent yield. Various linkers were introduced following a coupling reaction between 1-aminopyrene and corresponding long chain acid. In the final step, the

carbonyl group (both in amide and ester) was reduced by refluxing with borane in anhydrous tetrahydrofuran (Scheme 1).



**Scheme 1:** Synthesis of the pyrenyl derivatives (1-8)

Here it is important to be mentioned that in an earlier investigation [32] it was found that the anticancer activity of 3-carbon linker PAH derivatives was less than 5-carbon linker analogs. It was reported that 5-carbon linker PAH derivatives were more active anticancer agents than 3-carbon linker analogs but less active than 4-carbon linker analogs. Taken together, the activity of 3-, 4-, and 5-carbon linker PAH derivatives were as: 4-carbon linker > 5-carbon linker > 3-carbon linker. Based on this background information, the synthesis and anticancer screening of the corresponding 3-carbon linker pyrene analogs were excluded in the present investigation.

## 2.2. Biology

### 2.2.1. Virtual screening for druggability

The computed molecular properties of the *N*-pyrenyl derivatives (**1–8**) are presented in Table 1. The lipophilicity (fat-liking, miLogP), total polar surface area (TPSA), number of hydrogen bond acceptor, number of hydrogen bond donor, number of rotatable bonds and molecular volume have been calculated using Molinspiration online property calculation toolkit (version 2013.09) [35] to validate the druggability [36–38] of the pyrenyl derivatives (**1–8**). The drug-likeness model score (a collective property of physicochemical parameters, pharmacokinetics and pharmacodynamics of a compound is represented by a numerical value) has been calculated by MolSoft software [39]. The predicted bioactivities such as the ability of the pyrenyl compounds (**1–8**) to act as G protein-coupled receptor (GPCR) ligand, ion channel modulator, kinase inhibitor, nuclear receptor ligand, protease inhibitor and overall enzyme inhibitor have also been calculated using the same toolkit (version 2011.06) [35]. The results are summarized in Table 2.

### 2.2.2. Analysis of spectral emission

A previous study from our lab showed that either chrysenyl- or pyrenyl-coupled derivatives, including compounds **1** and **2**, exhibited autofluorescent properties whereby addition of an alkyl side chain to pyrene caused a red-shift in the spectral emission properties [15]. Therefore, to determine whether the novel pyrenyl derivatives described in Scheme 1 also exhibited autofluorescent properties, compounds were analyzed by fluorescence spectroscopy. Similar to compound **1** and **2**, compounds **6–8** exhibited peak fluorescent wavelengths ranging from 430 nm to greater than 450 nm, whereas the peak fluorescence of compounds **3–5** exhibited a peak

fluorescent wavelength of approximately 400 nm, (Ref 15, Figure 1 and Supplemental Figure 1 of this article). These data indicate that each of the novel pyrenyl derivatives with either piperidine or *N*-methyl piperazine exhibited autofluorescent properties, with the addition of the various long chains to pyrene causing a red-shift in spectral emission when compared to pyrene, since previous reports have identified that the peak emission wavelength of pyrene is less than 400 nm, with a shoulder for that emission peak at approximately 420 nm [40,41].

### 2.2.3. *In vitro* cytotoxicity evaluation

To determine whether the novel pyrenyl-coupled derivatives with side chains containing piperidine or *N*-methyl piperazine rings were cytotoxic, a small panel of cancer cell lines, including liver cells (HepG2 and Hepa1-6), colon cancer cells (HT-29 and Caco-2), a cervical cancer cell line (HeLa) and a breast cancer cell line (MCF-7) were treated with the eight novel compounds (**1-8**) described in Scheme 1. While two of the compounds, **3** and **4**, were not very cytotoxic, the other compounds exhibited cytotoxicity against each of the cell lines tested (Table 1). Furthermore, compounds **6** and **8** exhibited potent cytotoxicity against the cell lines tested with  $IC_{50}$  values of less than 5  $\mu$ M (Table 3). These data indicate that compound **6** and **8** are the most effective cytotoxic molecules of this set of pyrenyl derivatives, suggesting that having a 4-carbon linker is more effective than a 5-carbon linker (compare compound **6** with compound **7**) and that a more polar side chain is more effective than having hydrophilic groups such as ketones (compare compounds **6** and **8** with compounds **3** and **5**, respectively) present in the side chain. We also investigated the time at which the more potent compounds, **6** and **8**, caused cytotoxicity in cancer cells. Both compounds **6** and **8** caused cytotoxicity at a similar time-point in HepG2 cells when cells were treated with a dose that was two times greater than the  $IC_{50}$  value for the indicated cell type, causing toxicity between six and 12 hours of treatment (Figure 2).

### 2.2.4. *In vitro* evaluation of selective cytotoxicity

Upon identifying the cytotoxic pyrenyl derivatives containing piperidine or *N*-methyl piperazine rings, we sought to determine whether these compounds were selectively cytotoxic against a mouse cancer cell line (Hepa 1-6) *in vitro* when compared with normal hepatocytes. At very high doses (50  $\mu$ M), compound **6** and compound **8** killed both the cancer cells and the normal hepatocytes (Figure 2); however, at lower doses (less than 5  $\mu$ M) the pyrenyl compounds

killed the cancer cell line much more effectively when compared with the normal hepatocytes (Figure 2). These data suggest that pyrenyl derivatives containing a four carbon linker with either a piperidine or an *N*-methyl piperazine ring are capable of selectively killing certain cell types.

#### 2.2.5. Apoptosis through caspase-independent manner

To determine the mechanism by which compounds **6** and **8** caused cytotoxicity, the morphology of HeLa cells was examined for the presence of membrane blebbing, an indicator of cellular apoptosis. Membrane blebbing was detected in HeLa cells that were treated for 12 hours with either compound **6** or compound **8** (Figure 3A, white arrows), and similar morphology was detected when cells were treated for either 8 hours or 15 hours (data not shown). These data suggest that the cytotoxic pyrenyl-coupled derivatives containing a piperidine or an *N*-methyl piperazine ring cause cytotoxicity by apoptosis. However, there were also some cells with a rounded and swollen morphology in the presence of either compound **6** or compound **8**, suggesting that these cells were undergoing necrosis (Figure 3A, black arrows).

To further determine whether compound **6** or **8** was inducing apoptosis, we examined cleavage of poly (ADP-ribose) polymerase (PARP), a known proteolytic target of caspase proteins during progression of apoptosis [42]. Surprisingly, neither compound **6** nor **8** induced cleavage of PARP in cells that were treated with dosages less than 10  $\mu$ M for 8 to 18 hours (Figure 3B and data not shown). Only when cells were treated with higher doses of compounds (10  $\mu$ M) could a minimal level of cleaved PARP be detected (Figure 3B). These data suggest that most of the cytotoxicity induced by compound **6** or compound **8** occurs in a caspase-independent manner, even though the compounds are causing plasma membrane morphological changes.

#### 2.2.6. Localization to plasma membrane

Our group has previously shown that compound **2**, which is not as cytotoxic as compounds **6** or **8** (see Table 3), is localized outside the cell nucleus in a punctate pattern, when examined by epifluorescent microscopy [15]. To determine whether the cytotoxic pyrenyl-coupled derivatives containing a four carbon linker with either a piperidine or an *N*-methyl piperazine ring were capable of penetrating the cell and localizing to the nucleus, we compared the localization of these compounds by epifluorescent microscopy. Similar to our previous study, compound **2** exhibited a punctate pattern that was not localized to the nucleus (Figure 4A). Similarly,

compounds **6** and **8** exhibited a punctate pattern that appeared to be localized to the cytoplasmic membrane (Figure 4A). However, some diffuse staining could also be detected throughout the cell (Figure 4A), suggesting that some compound was getting into the nucleus. Therefore, we next analyzed the localization of compounds along with BODIPY TR-conjugated ceramide analogs, which localize to membrane fractions, by confocal microscopy. Each compound (**2**, **6**, and **8**) was detected in a punctate pattern that was predominantly co-localized with BODIPY TR-conjugated ceramide analogs, and the nucleus could be seen as an unstained component of the labeled cells (Figure 4B). Taken together, these data indicate that novel pyrenyl derivatives, whether highly cytotoxic or mildly cytotoxic, are localized to the membrane of cells.

Cells that were labeled with the fluorescent pyrenyl compounds and BODIPY TR-conjugated ceramide analogs were also subjected to biochemical fractionation using an OptiPrep<sup>TM</sup> density gradient. Both ceramide analogs and the pyrenyl compounds were predominantly detected in the less dense fractions (fractions 2–4), although some of the ceramide could be detected in heavier fractions (predominantly fractions 8–9) as well (Figure 5). Fractions were also analyzed by western blotting for two proteins that have previously been shown to localize to lipid rafts, Lyn and Thy-1 [43], as well as Glyceraldehyde Phosphate Dehydrogenase (GAPDH). Interestingly, Thy-1, which is a glycosylphosphatidylinositol (GPI)-anchored protein that binds to the outer membrane leaflet of cells [44], was detected in fractions that contained much of the pyrenyl compound as well as ceramide; however, both Lyn and GAPDH were detected in the denser fractions (Figure 5). These data suggest that these novel pyrenyl compounds are localized to the plasma membrane and are most likely located in inositol-rich regions within the membrane.

### 2.2.7. Circumvention of *P*-glycoprotein-mediated drug resistance

Because the cytotoxic pyrenyl derivatives containing a piperidine or an *N*-methyl piperazine ring (compound **6** and **8**, respectively) were localized to the cytoplasmic membrane and not to the cytoplasm, we hypothesized that these compounds might circumvent *P*-glycoprotein-mediated drug resistance in tumor cells. Therefore, cell viability of SKOV3 cells or a retrovirally transduced and subcloned SKOV3 cell line overexpressing *P*-Glycoprotein-1, SKOV3-MDR1-M6/6 [45,46] was assessed after treatment with low doses (0–4  $\mu$ M) or high doses (0–25  $\mu$ M) of Paclitaxel, 0–25  $\mu$ M compound **6**, or 0–25  $\mu$ M compound **8** for 48 hours. These SKOV3-MDR1-M6/6 cells have previously been shown to be resistant to cytotoxicity induced by anticancer

drugs, including Daunorubicin and Paclitaxel, when compared with SKOV3 cells [45,46]. As expected, SKOV3 cells were extremely susceptible to Paclitaxel-induced cell death, with an  $IC_{50}$  value of less than 1 nM (Figure 6A, left panel). In contrast, SKOV3-MDR1-6/6 displayed a clear resistance to Paclitaxel, which killed only 40% of cells, even at the highest dosage administered (Figure 6A and 6B, right panels). In contrast, the novel cytotoxic pyrenyl derivatives, compound **6** and **8**, killed SKOV3 and SKOV3-MDR1-6/6 cells similarly, having both a comparable  $IC_{50}$  value and maximum cell death percentage in each cell type (Figure 6C and 6D). This comparative cytotoxicity data indicates that these novel pyrenyl derivatives with either a piperidine or an *N*-methyl piperazine ring in their side chain bypasses the P-glycoprotein-mediated resistance of SKOV3-MDR1-M6/6 cells.

#### 2.2.8. Qualitative structure-activity relationship

Our group has previously shown that coupling of nitrated PAHs, including nitrated pyrene, with isobutyl chloroformate results in compounds that are autofluorescent and moderately cytotoxic against certain cancer cell lines [15]. In an effort to improve the cytotoxic potency of pyrenyl-coupled compounds, we have coupled side chains to nitrated pyrene that contain either piperidine or *N*-methyl piperazine in this study. We found that either piperidine (compound **6**) or *N*-methyl piperazine (compound **8**) coupled to nitrated pyrene through a four carbon linker lacking keto groups were most potent at causing cytotoxicity in cancer cells. We have also shown that these compounds can selectively ‘kill’ cancer cells when compared with primary cells and circumvent P-glycoprotein-mediated drug resistance in cancer cells *in vitro*, possibly because the mechanism of action for these molecules occurs through their interaction with the cellular membrane.

Other anticancer agents that contain either a piperidine or an *N*-methyl piperazine ring include Raloxifene (a selective estrogen receptor modulator), Imatinib (a tyrosine kinase inhibitor), and Bosutinib (a Src kinase inhibitor) [47–49]. In fact, the piperidine ring of Raloxifene is critical for its antagonistic effect on Estrogen Receptor activity [50]. The piperidine ring of Raloxifene is coupled to its adjacent benzene ring through an ester bond along with a 2-carbon linker [48], while the *N*-methyl piperazine of Imatinib or Bosutinib is linked through a 1-carbon or an ester along with a 3-carbon linker, respectively [47,49]. Our data indicate that a four carbon linker connecting piperidine to the pyrenyl backbone is more potent when compared to compounds

with a five carbon linker (Table 3; compare compound **6** with **7**) and that the presence of amide carbonyl groups in the linker severely reduces the efficacy of the compound (Table 3; compare compound **3** with **6** or compound **5** with **8**). These highly cytotoxic compounds were also selectively cytotoxic, killing rapidly growing cancer lines at much lower doses than non-dividing primary cells (Figure 2). Perhaps reducing the number of carbons in the linker between the piperidine or *N*-methyl piperazine ring and the pyrenyl backbone even further will render future compounds even more potent or selective.

Cytotoxicity can be caused through multiple processes, including apoptosis, apoptosis-like programmed cell death (e.g., autophagy, mitotic catastrophe, and paraptosis), necrosis, or necrosis-like programmed cell death [51]. A major difference between apoptosis and other types of cell death is that caspase proteins are activated during progression of apoptosis [51]. Both Raloxifene, which contains a piperidine moiety, and Imatinib, which contains an *N*-methyl piperazine moiety, have been shown to induce caspase activation in various cancer cell types, including HeLa cells [52–58]. In addition, a previous study has shown that pyrenyl coupled with a maleimide moiety causes cell death through caspase activation in T-cell leukemia-derived Jurkat cells [59]. However, the most potent cytotoxic compounds examined in this study (**6** and **8**) caused cellular membrane blebbing, which is indicative of apoptosis, but did not induce caspase activation in HeLa cells (Figure 3). These data suggest that pyrenyl-coupled cytotoxic agents may kill different cell types through different mechanisms or that the moiety that is coupled to the pyrenyl may change the cytotoxic mechanism of the compound. Furthermore, these data suggest that pyrenyl coupled with a side chain with either a piperidine or *N*-methyl piperazine ring causes caspase-independent cell death, which has been shown to occur when certain cancer cell types were treated with other types of cytotoxic agents including Cladribine, Paclitaxel, or Vitamin D [51]. Thus, it is possible that the novel cytotoxic pyrenyl-coupled compounds described here induce apoptosis-like programmed cell death, cellular necrosis, necrosis-like programmed cell death, or a combination of these cell death mechanisms. This is a plausible scenario, since Imatinib has previously been shown to induce cell death in leukemic cells through two separate mechanisms: (i) apoptosis and (ii) a caspase-independent, necrosis-like manner that was blocked by a serine protease inhibitor [60].

In addition to killing several different types of cancer cell lines, the novel pyrenyl-coupled compounds with either a piperidine ring (**6**) or an *N*-methyl piperazine (**8**) in the side chain were

both capable of circumventing the drug resistance in SKOV3-MDR1-M6/6 ovarian cancer cells overexpressing P-glycoprotein (Figure 6). These cells were previously shown to exhibit a robust resistance to Paclitaxel (Figure 6 and ref [46]). P-glycoprotein is one of nine Multidrug Resistant Proteins (MRPs), and MRPs are expressed in various tissues of the body and capable of transporting numerous physiological substrates or anticancer drugs out of cells [61]. Thus, it would be interesting to assess whether the pyrenyl-coupled compounds described here or additional pyrenyl-coupled compounds circumvented the multidrug resistance mediated by MDR1 and other MDR proteins *in vitro* and *in vivo*.

One possibility for the mechanism by which the novel pyrenyl-coupled compounds described here kill cancer cells potently and selectively, as well as circumvent the P-glycoprotein-mediated drug resistance, is that these compounds localize to the plasma membrane of target cells and do not enter the cytoplasm or intracellular organelles of the cell to cause cytotoxicity. Both compound **6** and **8** co-localized with a BODIPY-labeled sphingolipid at punctate regions on the cell surface when examined by microscopy (Figure 4) and in similar subcellular fractions when examined by biochemical fractionation of cells. These BODIPY-labeled sphingolipids have been reported to localize along the endocytic pathway, including the plasma membrane, endosomes, lysosomes, and the Golgi apparatus [62]. However, the lipid is primarily integrated in the plasma membrane when incubated at cold temperatures, as described here [62].

### 3. Conclusion

The cytotoxic pyrenyl-coupled compounds were primarily detected in cellular fractions containing the Thy-1 protein (CD90), a GPI-anchored protein found on the outer leaflet of the lipid bilayer [44], but not with GAPDH, an intracellular protein that has been shown to interact with phosphatidylserine [63]. Thus, our data suggest that the cytotoxic pyrenyl-coupled compounds are localized to the outer leaflet of the plasma membrane of target cells. However, the presence of pyrenyl-coupled cytotoxic compounds in endosomes or lysosomes cannot be ruled out by these results, since Thy-1 has been observed to localize at the plasma membrane and within endolysosomes [64]. Nonetheless, if these novel pyrenyl-coupled compounds potently and selectively kill cancer cells and circumvent drug resistance by binding to the plasma membrane or lysosome and causing a caspase-independent programmed cell death event, then they could become chemotherapeutic drugs with clinical usefulness.

## 4. Experimental

### 4.1. Chemistry

#### 4.1.1. General

Unless otherwise stated, all materials were obtained from commercially available sources and were used without purification. Pyrene, bismuth nitrate pentahydrate, montmorillonite KSF clay, indium, ammonium chloride, isobutyl chloroformate, 1.0 M borane in tetrahydrofuran, and dimethylsulfoxide (DMSO) were purchased from (Sigma-Aldrich Corporation, St. Louis, MO) while other solutions like phosphate-buffered saline (PBS), Dulbecco's Modified Eagle's Medium (DMEM), Fetal Bovine Serum (FBS), and McCoy's media were purchased from Invitrogen (Carlsbad, CA). All other chemicals were purchased from Sigma-Aldrich Corporation (analytical grade). Throughout the project solvents were purchased from Fisher-Scientific (Pittsburgh, PA). Deionized water was used for the preparation of all aqueous solutions.

Melting points were determined in a Fisher Scientific electrochemical Mel-Temp\* manual melting point apparatus (Model 1001) equipped with a 300°C thermometer. FT-IR spectra were registered on a Thermo Nicolet NEXUS 470 FT-IR E.S.P.<sup>TM</sup> spectrophotometer as KBr discs. <sup>1</sup>H-NMR (600 MHz) and <sup>13</sup>C-NMR (150 MHz) spectra were obtained at room temperature with Bruker superconducting Ultrashield<sup>TM</sup> Plus 600 MHz NMR spectrometer with central field 14.09 Tesla, coil inductance 89.1 Henry and magnetic energy 1127.2 kJ using CDCl<sub>3</sub> as solvent. Elemental analyses (C, H, N) were conducted using the Perkin-Elmer 2400 series II elemental analyzer, their results were found to be in good agreement ( $\pm 0.2\%$ ) with the calculated values for C, H, N.

#### 4.1.2. Synthesis of the compounds 1–8

##### 4.1.2.1. Nitration of pyrene

Pyrene (1 mmol) and montmorillonite KSF clay (500 mg, Aldrich) were added to a suspension of bismuth nitrate pentahydrate (1 equiv.) in anhydrous dichloromethane (10 mL). The solvent was then evaporated under reduced pressure and the reaction mixture was irradiated using microwave irradiation for 6 min (2x3 min). A 500 mL glass beaker full with ice was used as heat sink. Every after 2 min the reaction was monitored by TLC. After completion of the

reaction the reaction mixture was washed with dichloromethane (3x 5mL) and the solvent was evaporated by reduced pressure distillation. The pure product (1-nitropyrene) was isolated by crystallization from dichloromethane/hexanes mixture in excellent yield (~ 80%).

#### 4.1.2.2. Reduction of 1-nitropyrene to the 1-aminopyrene

1-Nitropyrene (1 mmol) and indium (570 mg), 2.5 mL ethanol and 2.5 mL 20% aqueous ammonium chloride solution was refluxed vigorously for 24 hrs (monitored by TLC). After completion of the reaction it was filtered through Büchner funnel and the filtrate was extracted with dichloromethane (2x 3 mL). The dichloromethane layer was washed with brine and water successively and dried over anhydrous sodium sulfate. The pure amine was isolated by crystallization from dichloromethane/hexanes mixture in excellent yield (86%).

#### 4.1.2.3. Synthesis of the acidic chains

The anhydride (n=1, succinic anhydride and n=2, glutaric anhydride) and piperidine (1:1 molar ratio) were dissolved in anhydrous dichloromethane (10 mL) and the mixture was refluxed for 4—6 hrs; cooled down at room temperature. The crystals were filtered through vacuum, washed successively with diethyl ether and hexanes and dried in desiccator.

#### 4.1.2.4. Coupling of 1-aminopyrene with the acidic chains in the presence of isobutyl chloroformate

1-Aminopyrene (1 mmol) was stirred with dry triethylamine (3 mmol) in anhydrous dichloromethane (5 mL) at a temperature -5 to 0°C and isobutyl chloroformate (1.8 mmol in 2 mL anhydrous dichloromethane) was added drop wise during an hour. After the addition was over, the mixture was stirred for 24 hours at room temperature. After completion of the reaction (monitored by TLC), the mixture was washed with saturated solution of sodium bicarbonate, brine and water successively. The pure product was isolated after column chromatography over silica gel (>70% yield).

#### 4.1.2.5. Reduction of the diamides (3—5) to diamines (4—6)

1 mmol of the diamide was refluxed with 6 mL of 1.0 M borane/tetrahydrofuran solution for 36 hours and then 5 mL of 4% aqueous hydrochloric acid solution was added and the mixture

was again refluxed for another 24 hrs. After completion of the reaction (monitored by TLC), the pH of the solution was changed to ~7.0 by 10% aqueous sodium hydroxide solution and the mixture was extracted with ethyl acetate for three times (3x3 mL). The combined organic layer was washed with brine and water successively. The pure diamine was isolated after column chromatography (10% methanolic ethyl acetate) over silica gel (~70% yield).

#### 4.1.2.6. Reduction of (1) to (2):

Compound (1) was formed as a byproduct during diamide synthesis. Following the previous protocol of diamide reduction it was reduced to compound (2) and finally purified by column chromatography (15% ethyl acetate in hexanes) over silica gel (~60% yield).

#### 4.1.2.7. Spectroscopic data for characterization of the compounds

The spectral and analytical data of the compounds **1** and **2** are already reported [15] from our laboratory. The data for the compounds (**3–8**) are as follows:

4.1.2.7.1. *4-Oxo-4-(piperidin-1-yl)-N-(pyren-4-yl)butanamide (3)*: Brown crystalline solid (74%); mp 163–164 °C; IR (KBr) 3265, 2926, 1670, 1624, 1508, 838, 711 cm<sup>-1</sup>; <sup>1</sup>H NMR (600 MHz, CDCl<sub>3</sub>) δ 1.46 (m, 6H), 2.75 (t, *J* = 6.36 Hz, 2H), 2.89 (t, *J* = 5.70 Hz, 2H), 3.32 (m, 2H), 3.56 (t, *J* = 5.40 Hz, 2H), 7.98 (m, 7H), 8.14 (d, *J* = 9.18 Hz, 1H), 8.44 (d, *J* = 8.28 Hz, 1H), 9.59 (s, 1H); <sup>13</sup>C NMR (150 MHz, CDCl<sub>3</sub>) 26.41, 25.60, 26.29, 29.70, 33.08, 43.22, 46.51, 120.92, 121.41, 122.88, 124.69, 124.81, 125.09 (2C), 125.16, 125.97, 126.39, 127.36, 127.52, 128.49, 130.91 (2C), 131.39, 170.50, 171.99. Anal. Calcd for C<sub>25</sub>H<sub>24</sub>N<sub>2</sub>O<sub>2</sub>: C, 78.10; H, 6.29; N, 7.29. Found: C, 78.01; H, 6.23; N, 7.20.

4.1.2.7.2. *5-Oxo-5-(piperidin-1-yl)-N-(pyren-4-yl)pentanamide (4)*: White amorphous solid (71%); mp 102-104 °C; IR (KBr) 3232, 2933, 1685, 1647, 1555, 1521, 1437, 1266, 843, 710 cm<sup>-1</sup>; <sup>1</sup>H NMR (600 MHz, CDCl<sub>3</sub>) δ 1.53 (m, 8H), 2.07 (q, *J* = 6.84, 13.62 Hz, 2H), 2.59 (t, *J* = 6.96 Hz, 2H), 3.40 (t, *J* = 7.02 Hz, 2H), 3.52 (t, *J* = 5.34 Hz, 2H), 7.87 (t, *J* = 7.56 Hz, 2H), 7.91 (d, *J* = 10.56 Hz, 1H), 8.02 (m, 4H), 8.12 (d, *J* = 9.12 Hz, 1H), 8.32 (d, *J* = 8.22 Hz, 1H), 9.06 (s, 1H); <sup>13</sup>C NMR (150 MHz, CDCl<sub>3</sub>) 21.85, 24.49, 25.65, 26.59, 32.12, 36.68, 42.83, 46.82, 120.87, 121.99, 123.37, 124.75, 124.80, 125.11 (2C), 125.17, 126.00, 126.56, 127.32, 127.65, 128.78, 130.88, 131.06, 131.35, 171.02, 172.21. Anal. Calcd for C<sub>26</sub>H<sub>26</sub>N<sub>2</sub>O<sub>2</sub>: C, 78.36; H, 6.58; N, 7.03. Found: C, 78.17; H, 6.41; N, 7.09.

4.1.2.7.3. *4-(4-Methylpiperazin-1-yl)-4-oxo-N-(pyren-4-yl)butanamide (5)*: Brownish white amorphous solid (68%); mp 160–161 °C; IR (KBr) 3289, 2929, 1646, 1555, 1526, 1429, 1287, 1007, 831, 705 cm<sup>-1</sup>; <sup>1</sup>H NMR (600 MHz, CDCl<sub>3</sub>) δ 1.91 (broad s, 1H), 2.27 (s, 3H), 2.37 (m, 3H), 2.86 (m, 2H), 3.00 (m, 2H), 3.50 (broad s, 2H), 3.73 (broad s, 2H), 7.99 (m, 3H), 8.06 (d, *J* = 9.00 Hz, 1H), 8.15 (m, 3H), 8.21 (d, *J* = 9.06 Hz, 1H), 8.50 (d, *J* = 7.92 Hz, 1H), 9.48 (s, 1H); <sup>13</sup>C NMR (150 MHz, CDCl<sub>3</sub>) 29.49, 32.84, 41.98, 45.30, 45.95, 54.61, 54.88, 120.83, 121.60, 123.05, 124.77, 125.15 (2C), 126.02, 126.50, 127.34, 127.60, 128.63, 130.87, 131.18, 131.37, 170.73, 171.76. Anal. Calcd for C<sub>25</sub>H<sub>25</sub>N<sub>3</sub>O<sub>2</sub>: C, 75.16; H, 6.31; N, 10.52. Found: C, 75.01; H, 6.40; N, 10.37.

4.1.2.7.4. *N-(4-(piperidin-1-yl)butyl)pyren-4-amine (6)*: Yellowish green crystalline solid (69%); mp 184–185 °C; IR (KBr) 3339, 2933, 1601, 1528, 1283, 839, 724 cm<sup>-1</sup>; <sup>1</sup>H NMR (600 MHz, d<sub>6</sub>-DMSO) δ 1.34 (m, 1H), 1.80 (m, 8H), 3.01 (m, 3H), 3.20 (t, *J* = 7.56 Hz, 1H), 3.26 (dd, *J* = 6.48 Hz, 1H), 3.41 (m, 4H), 6.85 (t, *J* = 5.40 Hz, 1H), 7.05 (d, *J* = 8.70 Hz, 1H), 7.32 (m, 1H), 7.44 (m, 1H), 7.64 (m, 1H), 7.88 (m, 1H), 8.01 (m, 1H), 8.05 (d, *J* = 8.46 Hz, 1H), 8.46 (d, *J* = 9.30 Hz, 1H), 10.63 (s, 1H); <sup>13</sup>C NMR (150 MHz, d<sub>6</sub>-DMSO) 20.89, 21.44, 22.21, 25.57, 27.50, 42.40, 51.74, 51.77, 55.48, 108.20, 115.52, 121.10, 121.64, 121.95, 122.51, 122.97, 124.40, 125.08, 125.54, 125.95, 126.75, 127.74, 131.52, 132.08, 143.51. Anal. Calcd for C<sub>25</sub>H<sub>28</sub>N<sub>2</sub>: C, 84.23; H, 7.92; N, 7.86. Found: C, 84.04; H, 7.86; N, 7.77.

4.1.2.7.5. *N-(5-(piperidin-1-yl)pentyl)pyren-4-amine (7)*: Brown solid (67%); mp 65–67 °C; IR (KBr) 3347, 2928, 1620, 1525, 1461, 1266, 1042, 759 cm<sup>-1</sup>; <sup>1</sup>H NMR (600 MHz, d<sub>6</sub>-DMSO) δ 1.40 (m, 12H), 1.63 (m, 1H), 2.20 (m, 4H), 2.98 (t, *J* = 8.16 Hz, 1H), 3.20 (m, 2H), 7.03 (d, *J* = 8.64 Hz, 1H), 7.28 (d, *J* = 8.46 Hz, 1H), 7.32 (d, *J* = 7.02 Hz, 1H), 7.39 (d, *J* = 8.76 Hz, 1H), 7.44 (t, *J* = 7.26 Hz, 1H), 7.58 (d, *J* = 8.76 Hz, 1H), 7.67 (m, 1H), 7.87 (m, 1H), 7.98 (m, 1H), 8.39 (d, *J* = 9.30, 1H); <sup>13</sup>C NMR (150 MHz, d<sub>6</sub>-DMSO) 23.23, 24.20, 24.81, 26.31, 27.52, 28.86, 29.78, 43.26, 54.10, 58.66, 108.14, 112.00, 114.67, 121.81, 122.12, 122.40, 126.08, 126.32, 126.65, 126.74, 126.86, 127.74, 128.10, 128.62, 134.33, 143.79. Anal. Calcd for C<sub>26</sub>H<sub>30</sub>N<sub>2</sub>: C, 84.28; H, 8.16; N, 7.56. Found: C, 84.13; H, 8.04; N, 7.39.

4.1.2.7.6. *N-(4-(4-methylpiperazin-1-yl)butyl)pyren-4-amine (8)*: Dark green solid (64%); mp 72–73 °C; IR (KBr) 3403, 2925, 2783, 1593, 1515, 1441, 1277, 1162, 1131, 1001, 820, 756, 732 cm<sup>-1</sup>; <sup>1</sup>H NMR (600 MHz, d<sub>6</sub>-DMSO) δ 1.53 (m, 2H), 1.64 (m, 2H), 2.28 (s, 3H), 2.30 (m, 7H), 2.98 (t, *J* = 7.80 Hz, 2H), 3.38 (m, 3H), 7.06 (d, *J* = 8.52 Hz, 1H), 7.32 (m, 1H), 7.39 (d, *J* =

8.70 Hz, 1H), 7.44 (t,  $J = 7.32$  Hz, 1H), 7.59 (d,  $J = 8.64$  Hz, 1H), 7.64 (dd,  $J = 10.74, 3.84$  Hz, 2H), 7.88 (m, 1H), 8.00 (m, 1H), 8.39 (d,  $J = 9.30$ , 1H);  $^{13}\text{C}$  NMR (150 MHz,  $\text{d}_6\text{-DMSO}$ ) 21.36, 23.96, 26.76, 27.52, 43.14, 45.77, 52.70, 54.80, 57.52, 112.08, 114.68, 121.06, 122.12, 123.89, 125.20, 126.09, 126.31, 126.65, 126.87, 128.10, 131.03, 134.35, 143.78. Anal. Calcd for  $\text{C}_{25}\text{H}_{29}\text{N}_3$ : C, 80.82; H, 7.87; N, 11.31. Found: C, 80.70; H, 7.71; N, 11.27.

## 4.2. Biology

### 4.2.1. Mammalian cell culture and viability assays

HepG2, Hepa1-6, HeLa, and MCF-7 cells were cultured in Dulbecco's Modified Eagle's Medium (DMEM) (Invitrogen, Carlsbad, CA) containing 10% Fetal Bovine Serum (FBS, Invitrogen); Caco-2 cells were cultured in DMEM containing 20% FBS, and HT-29 cells were cultured in McCoy's media (Invitrogen) containing 10% FBS. SKOV3, and SKOV3-MDR1-M6/6 cells were grown in Basal Medium Eagle (BME) media containing 10% FBS. All cell lines were purchased from American Type Culture Collection (ATCC, Manassas, VA) except for MCF-7, which were provided by Dr. R.K. Dearth (UTPA), as well as SKOV3 and SKOV3-MDR1-M6/6 cells, which were provided by Dr. Susan Mooberry (UTHSCSA). All cells were incubated at  $37^\circ\text{C}$  with 5%  $\text{CO}_2$ . Cell viability assays were performed as described previously [15], and  $10\text{-}\mu\text{M}$  doxorubicin was used as a positive control for cytotoxicity.

### 4.2.2. Spectral analysis of the compounds (1–8)

The autofluorescent properties of compounds (2-8) were analyzed as described previously [15]. Briefly, each compound was excited with light at a wavelength of 350 nm, and the subsequent light emission was analyzed between the wavelengths of 350-700 nm using a SpectraMaxM5 plate reader (Molecular Devices, Sunnyvale, CA).

### 4.2.3. Apoptosis assays

To detect membrane blebbing, HeLa cells were plated onto 6-well dishes at a density of  $1.5\text{-}2.0 \times 10^5$  cells/well. Cells were then treated with the compound **6** or **8** at the indicated dosages and visualized after 12 hrs using an Olympus CKX31 culture microscope (Olympus Corp., Tokyo, Japan). Images were captured using a Nikon Coolpix E995 eyepiece camera (Nikon, Japan).

For PARP cleavage, HeLa cells were treated with the indicated dosages of compound **6** or **8** for 12-hrs, and cells were lysed using 0.5% SDS-Lysis Buffer (50mM Tris - pH 8.0, 0.5% SDS, 1mM DTT, 2.5mM sodium pyrophosphate, 1mM  $\beta$ -glycerophosphate, 1mM  $\text{Na}_3\text{VO}_4$ , and 1X Roche Complete Protease Inhibitors). Lysates were analyzed by western blotting using an anti-PARP antibody (Cell Signaling Technology, Danvers, MA), and Staurosporine was used as a positive control for PARP cleavage.

#### 4.2.4. Subcellular localization

For localization of compounds, HepG2 cells were plated onto 6-well dishes (250,000 cells/well) containing 12-mm glass cover slips and incubated overnight at 37°C. The following day, experimental groups were treated with compound **2** (50 $\mu\text{M}$ ) for 4 hrs, or with compound **6** or **8** (30 $\mu\text{M}$ ) for 3 hours. Treated cells were then fixed and visualized as described previously [15]. Briefly, treated cells were visualized using a Zeiss AxioImager.Z1 epifluorescent microscope (Carl Zeiss Microimaging, LLC, Thornwood, NY) with EGFP (Excitation – 470/40; Emission – 525/50) and DAPI filters, and images were acquired using AxioVision Rel. 4.6 software (Zeiss).

For co-localization of compounds with ceramide, cells (200,000 cells/well) were plated onto 12-well dishes (Costar) containing 12-mm glass cover slips and incubated overnight at 37°C. The following day, experimental groups were treated with compound **2** (50  $\mu\text{M}$ ) for 4 hrs or with compound **6** or **8** for 3 hours. After treatment, cells were rinsed several times with PBS containing powdered Bovine Serum Albumin (BSA) (0.34 mg/mL) and then stained with 5- $\mu\text{M}$  BODIPY TR-labeled sphingolipids (Molecular Probes) for 30 minutes at 4°C. Cells were then fixed with PBS containing 4% paraformaldehyde for 25 minutes at room temperature and permeabilized using PBS containing 0.2% Triton-X-100 for 5 minutes at room temperature. Coverslips were then mounted onto glass slides using ProLong Gold Antifade mounting media (Invitrogen) and visualized using an Olympus Fluoview FV1000 Confocal microscope (Olympus America Inc. Center Valley, PA, USA) with Cyanine 3.5 (Excitation – 543; Emission - 592) and AlexaFluor405 (Excitation – 405; Emission - 415/75) channels engaged. Z-stacked composites were generated across a 10  $\mu\text{m}$  field at 1 $\mu\text{m}$  increments under 60x oil immersed objective magnification and 4.0 digital zoom.

#### 4.2.5. Biochemical fractionation

HepG2 cells were plated onto 10-cm dishes ( $1 \times 10^6$  cells/plate) and incubated overnight at 37° C. The following day, cells were treated with compound **2** (5 $\mu$ M) for 4 hrs, or cells were treated with compound **6** or **8** (3 $\mu$ M) for 2 hrs. After treatment, plates were washed with PBS containing defatted BSA and stained with 5- $\mu$ M BODIPY TR-labeled sphingolipids (Molecular Probes) for 30 min at 4° C. After exposure to modified sphingolipids, cells were scraped from plates in PBS containing 1X Protease Inhibitors (Roche) and pelleted by centrifugation for 5 min at 3,000 x g. After thorough washing, cells were lysed with PBS containing 0.5% Brij-96 and protease inhibitors for one hour. Protein lysates were then quantified by Bicinchoninic Acid Assay (BCA) and normalized. Equal mass of protein lysate (600  $\mu$ L) for each treatment was then loaded onto a density gradient composed of 600- $\mu$ L step-wise gradients (2.5%, 10%, 20%, and 30 %) of OptiPrep (Sigma), and then separated by ultra-centrifugation at 125,000 g for 12 hrs with no braking. Equal volume fractions (300  $\mu$ L) were then collected from the density gradient, and a portion of each fraction was analyzed by spectral analysis using a SpectraMax M5 Spectrophotometer (Molecular Devices) to detect both compounds (Ex. 350 nm /Em. 450 nm) and BODIPY TR-labeled sphingolipids (Ex. 589 nm; Em. 617 nm) in each fraction. In addition, a portion of each fraction collected was used for western blotting analysis using an antibody for Lyn or Thy-1 (Cell Signaling Technology), or an antibody for GAPDH (Santa Cruz Biotech.).

#### Acknowledgments

We gratefully acknowledge the funding support from National Cancer Institute (NIH/NCI-P20, Grant# 5P20CA138022-02) and Kleberg Foundation of Texas.

#### Supporting data

The following information can be found online: (i) The fluorescence emission spectra of three compounds (**4**, **5**, and **7**), (ii) the time-course for compounds **6** and **8** causing cytotoxicity of HepG2 cells, and (iii) the infrared (IR), proton magnetic resonance (PMR) and carbon magnetic resonance (CMR) spectra of the compounds **3–8**.

#### References

[1] <http://www.nasa.gov/ames/need-to-track-organic-nano-particles-across-the-universe-nasas-got-an-app-for-that> (Accessed on June 28, 2014).

- [2] J.C. Fetzer, The chemistry and analysis of the large polycyclic aromatic hydrocarbons, *Polycycl. Aromat. Comp.* 27 (2000) 143–162.
- [3] G.M. Roy, Activated carbon applications in the food and pharmaceutical industries, Technomic Publishing Company Inc., Pennsylvania, 1995, p. 125.
- [4] A. Luch, The carcinogenic effects of polycyclic aromatic hydrocarbons. Imperial College Press, London, 2005.
- [5] B.K. Banik, F.F. Becker, Synthesis, electrophilic substitution and structure-activity relationship studies of polycyclic aromatic compounds towards the development of anticancer agents, *Curr. Med. Chem.* 8 (2001) 1513–1533.
- [6] [http://en.wikipedia.org/wiki/Polycyclic\\_aromatic\\_hydrocarbon](http://en.wikipedia.org/wiki/Polycyclic_aromatic_hydrocarbon) (Accessed on June 28, 2014).
- [7] V.T. De Vita, S. Hellman, S.A. Rosenberg, *Cancer: Principles and Practice of Oncology*, Sixth ed., Lippincott Williams and Wilkins: Philadelphia, Pennsylvania, 2001.
- [8] J.W. Lown, Anthracycline and anthraquinone anticancer agents: current status and recent developments, *Pharmacol. Ther.* 60 (1993) 185–214.
- [9] M.F. Brana, M. Cacho, A. Gradillas, B. de Pascual-Teresa, A. Ramos, Intercalators as anticancer drugs, *Curr. Pharm. Des.* 7 (2001) 1745–1780.
- [10] R. Martinez, L. Chacon-Garcia, The search of DNA-intercalators as antitumoral drugs: What it worked and what did not work, *Curr. Med. Chem.* 12 (2005) 127–151.
- [11] H. Malonne, G. Atassi, DNA topoisomerase targeting drugs: Mechanisms of action and perspectives, *Anti-Cancer Drugs* 8 (1997) 811–822.
- [12] <http://www.who.int/mediacentre/factsheets/fs297/en> (Accessed on July 03, 2014).
- [13] [http://globocan.iarc.fr/Pages/fact\\_sheets\\_cancer.aspx](http://globocan.iarc.fr/Pages/fact_sheets_cancer.aspx) (Accessed on July 03, 2014).
- [14] V. Fodale, M. Pierobon, L. Liotta, E. Petricoin, Mechanism of cell adaptation: When and how do cancer cells develop chemoresistance? *Cancer J.* 17 (2011) 89–95.
- [15] D. Bandyopadhyay, J.C. Granados, J.D. Short, B.K. Banik, Polycyclic aromatic compounds as anticancer agents: Evaluation of synthesis and *in vitro* cytotoxicity, *Oncol. Lett.* 3 (2012) 45–49.
- [16] L. Canales, D. Bandyopadhyay, B.K. Banik, Bismuth nitrate pentahydrate-induced novel nitration of Eugenol, *Org. Med. Chem. Lett.* 1 (2001) Article# 9.

- [17] D. Bandyopadhyay, G. Rivera, J.L. Sanchez, J. Rivera, J.C. Granados, A.M. Guerrero, F.-M. Chang, R.K. Dearth, J.D. Short, B.K. Banik, Bismuth nitrate-induced novel nitration of estradiol: An entry to new anticancer agents, *Eur. J. Med. Chem.* 82 (2014) 574–583.
- [18] D. Bandyopadhyay, S. Mukherjee, J.C. Granados, J.D. Short, B.K. Banik, Ultrasound-assisted bismuth nitrate-induced green synthesis of novel pyrrole derivatives and their biological evaluation as anticancer agents, *Eur. J. Med. Chem.* 50 (2012) 209–215.
- [19] S. Rivera, D. Bandyopadhyay, B.K. Banik, Facile synthesis of *N*-substituted pyrroles via microwave-induced bismuth nitrate-catalyzed reaction under solventless conditions, *Tetrahedron Lett.* 50 (2009) 5445–5448.
- [20] D. Bandyopadhyay, J. Cruz, B.K. Banik, Novel synthesis of 3-pyrrole substituted  $\beta$ -lactams via microwave-induced bismuth nitrate-catalyzed reaction, *Tetrahedron* 68 (2012) 10686–10695.
- [21] D. Bandyopadhyay, E. Rhodes, B.K. Banik, A green, chemoselective, and practical approach toward *N*-(2-azetidinyloxy) 2,5-disubstituted pyrroles, *RSC Adv.* 3, (2013) 16756–16764.
- [22] L. Iglesias, C. Aguilar, D. Bandyopadhyay, B.K. Banik, A new bismuth nitrate-catalyzed electrophilic substitution of indoles with carbonyl compounds under solventless conditions, *Synth. Commun.* 40 (2010) 3678–3682.
- [23] A. Banik, S. Bhatta, D. Bandyopadhyay, B.K. Banik, A highly efficient bismuth salts-catalyzed route for the synthesis of  $\alpha$ -aminophosphonates, *Molecules* 15 (2010) 8205–8213.
- [24] D. Bandyopadhyay, S. Maldonado, B.K. Banik, Microwave-assisted bismuth nitrate-catalyzed unique route toward 1,4-dihydropyridines, *Molecules* 17 (2012) 2643–2662.
- [25] D. Bandyopadhyay, J. Cruz, L.D. Morales, H.D. Arman, E. Cuate, Y.S. Lee, B.K. Banik, D.J. Kim, A green approach toward quinoxalines and bis-quinoxalines and their biological evaluation against A431, human skin cancer cell lines, *Future Med. Chem.* 5 (2013) 1377–1390.
- [26] D. Bandyopadhyay, S. Samano, J.C. Villalobos-Rocha, L.E. Sanchez-Torres, B. Nogueira-Torres, G. Rivera, B.K. Banik, A practical green synthesis, and biological evaluation of benzimidazoles against two neglected tropical diseases: Chagas and leishmaniasis, *Curr. Med. Chem.* **2014** (*in press*).
- [27] D. Bandyopadhyay, B.K. Banik, Microwave-induced stereoselectivity of  $\beta$ -lactam formation with dihydrophenanthrenyl imines via Staudinger cycloaddition, *Helv. Chim. Acta*, 93 (2010) 298–301.

- [28] D. Bandyopadhyay, G. Rivera, I. Salinas, H. Aguilar, B. K. Banik, Iodine-catalyzed remarkable synthesis of novel *N*-polyaromatic  $\beta$ -lactams bearing pyrroles, *Molecules* 15 (2010) 1082–1088.
- [29] D. Bandyopadhyay, S. Mukherjee, B.K. Banik, An expeditious synthesis of *N*-substituted pyrroles via microwave-induced iodine-catalyzed reaction under solventless conditions, *Molecules* 15 (2010) 2520–2525.
- [30] D. Bandyopadhyay, S. Mukherjee, R.R. Rodriguez, B.K. Banik, An effective microwave-induced iodine-catalyzed method for the synthesis of quinoxalines via condensation of 1,2-dicarbonyl compounds, *Molecules* 15 (2010) 4207–4212.
- [31] F. F. Becker, B.K. Banik, Polycyclic aromatic compounds as anticancer agents: Synthesis and biological evaluation of some chrysene derivatives, *Bioorg. Med. Chem. Lett.* 8 (1998) 2877–2880.
- [32] B.K. Banik, F.F. Becker, Polycyclic aromatic compounds as anticancer agents. 4. Structure-activity relationships of chrysene and pyrene derivatives, *Bioorg. Med. Chem.* 9 (2001) 593–605.
- [33] B.K. Banik, F.F. Becker, Novel 6,12-disubstituted chrysene as potent anticancer agent: Synthesis, in vitro and in vivo study, *Eur. J. Med. Chem.* 45 (2010) 4687–4691.
- [34] <http://www.atsdr.cdc.gov/csem/pah/docs/pah.pdf> (p.35, accessed on June 28, 2014).
- [35] Molinspiration Cheminformatics, Bratislava, Slovak Republic, available from: <http://www.molinspiration.com/cgi-bin/properties> (Accessed on July 04, 2014).
- [36] C.A. Lipinski, F. Lombardo, B.W. Dominy, P.J. Feeney, Experimental and computational approaches to estimate solubility and permeability in drug discovery and development settings, *Adv. Drug. Deliv. Rev.* 46 (2001) 3–26.
- [37] D.F. Veber, S.R. Johnson, H.-Y. Cheng, B.R. Smith, K.W. Ward, K.D. Kopple, Molecular properties that influence the oral bioavailability of drug candidates, *J. Med. Chem.* 45 (2002) 2615–2623.
- [38] P. Ertl, B. Rohde, P. Selzer, Fast calculation of molecular polar surface area as a sum of fragment-based contributions and its application to the prediction of drug transport properties, *J. Med. Chem.* 43 (2000) 3714–3717.
- [39] Drug-likeness and molecular property prediction from Molsoft LLC, San Diego, USA, available from: <http://www.molsoft.com/mprop/>; <http://www.molsoft.com/mprop/mprop.cgi>; <http://www.molsoft.com/mpropdesc.html> (Accessed on July 04, 2014).

- [40] L. Búcsiová, P. Hrdlovič, S. Chmela, Spectral characteristics of fluorescence probes based on pyrene in solution and in polymer matrix, *J. Photochem. Photobiol. A Chem.* 143 (2001) 59–68.
- [41] P. Hrdlovič, S. Chmela, Spectral characteristics of probes based on ionic derivatives of pyrene in polar polymer matrices, *J. Photochem. Photobiol. A Chem.* 118 (1998) 137–142.
- [42] C. Soldani, A.I. Scovassi, Poly(ADP-ribose) polymerase-1 cleavage during apoptosis: An update, *Apoptosis* 7 (2002) 321–328.
- [43] G. Radeva, F.J. Sharom, Isolation and characterization of lipid rafts with different properties from RBL-2H3 (rat basophilic leukaemia) cells, *Biochem. J.* 380 (2004) 219–230.
- [44] T.A. Rege, J.S. Hagood, Thy-1 as a regulator of cell-cell and cell-matrix interactions in axon regeneration, apoptosis, adhesion, migration, cancer, and fibrosis. *FASEB J.* 20 (2006) 1045–1054.
- [45] D. Sadava, A. Coleman, S.E. Kane, Liposomal daunorubicin overcomes drug resistance in human breast, ovarian and lung carcinoma cells, *J. Liposome Res.* 12 (2002) 301–309.
- [46] A.L. Risinger, E.M. Jackson, L.A. Polin, G.L. Helms, D.A. LeBoeuf, P.A. Joe, E. Hopper-Borge, R.F. Ludueña, G.D. Kruh, S.L. Mooberry, The taccalonolides: Microtubule stabilizers that circumvent clinically relevant taxane resistance mechanisms. *Cancer Res.* 68 (2008) 8881–8888.
- [47] F. Boschelli, K. Arndt, C. Gambacorti-Passerini, Bosutinib: A review of preclinical studies in chronic myelogenous leukaemia, *Eur. J. Cancer* (2010) 46, 1781–1789.
- [48] M. Heringa, Review on raloxifene: Profile of a selective estrogen receptor modulator, *Int. J. Clin. Pharmacol. Ther.* 41 (2003) 331–345.
- [49] P.W. Manley, S.W. Cowan-Jacob, E. Buchdunger, D. Fabbro, G. Fendrich, P. Furet, T. Meyer, J. Zimmermann, Imatinib: a selective tyrosine kinase inhibitor, *Eur. J. Cancer* 38 (Suppl 5) (2002) S19–27.
- [50] H. Liu, W.C. Park, D.J. Bentrem, K.P. McKian, A. De Los Reyes, J.A. Loweth, J.M. Schafer, J.W. Zapf, V.C. Jordan, Structure-function relationships of the raloxifene-estrogen receptor- $\alpha$  complex for regulating transforming growth factor- $\alpha$  expression in breast cancer cells, *J. Biol. Chem.* 277 (2002) 9189–9198.
- [51] L.E. Broker, F.A.E. Kruyt, G. Giaccone, Cell death independent of caspases: A review. *Clin. Cancer Res.* 11 (2005) 3155–3162.

- [52] K.L. Hoffman, S.P. Lerner, C.L. Smith, Raloxifene inhibits growth of RT4 urothelial carcinoma cells via estrogen receptor-dependent induction of apoptosis and inhibition of proliferation, *Horm. Cancer* 4 (2013) 24–35.
- [53] M. Obrero, D.V. Yu, D.J. Shapiro, Estrogen receptor-dependent and estrogen receptor-independent pathways for tamoxifen and 4-hydroxytamoxifen-induced programmed cell death, *J. Biol. Chem.* 277 (2002) 45695–45703.
- [54] S. Morishima, M. Shibata, M. Ohmichi, Y. Otsuki, Raloxifene, a selective estrogen receptor modulator, induces mitochondria-mediated apoptosis in human endometrial carcinoma cells, *Med. Mol. Morphol.* 41 (2008) 132–138.
- [55] I.Y. Kim, B. Kim, D.H. Seong, D.K. Lee, J. Seo, Y.J. Hong, H. Kim, R.A. Morton, S. Kim, Raloxifene, a mixed estrogen agonist/antagonist, induces apoptosis in androgen-independent human prostate cancer cell lines, *Cancer Res.* 62 (2002) 5365–5369.
- [56] O. Uziel, E. Fenig, J. Nordenberg, E. Beery, H. Reshef, J. Sandbank, M. Birenbaum, M. Bakhanashvili, R. Yerushalmi, D. Luria, M. Lahav, Imatinib mesylate (Gleevec) downregulates telomerase activity and inhibits proliferation in telomerase-expressing cell lines, *Br. J. Cancer* 92 (2005) 1881–1891.
- [57] K. Kuželová, M. Pluskalová, D. Grebenová, K. Pavlásková, P. Halada, Z. Hrkal, Changes in cell adhesivity and cytoskeleton-related proteins during imatinib-induced apoptosis of leukemic JURL-MK1 cells, *J. Cell. Biochem.* 111 (2010) 1413–1425.
- [58] Y. Liu, M. Tseng, S.A. Perdreau, F. Rossi, C. Antonescu, P. Besmer, J.A. Fletcher, S. Duensing, A. Duensing, Histone H2AX is a mediator of gastrointestinal stromal tumor cell apoptosis following treatment with imatinib mesylate, *Cancer Res.* 67 (2007) 2685–2692.
- [59] P. Huang, Y. Yeh, C. Pao, C. Chen, T.V. Wang, *N*-(1-Pyrenyl) maleimide inhibits telomerase activity in a cell free system and induces apoptosis in Jurkat cells, *Mol. Biol. Rep.* 39 (2012) 8899–8905.
- [60] M. Okada, S. Adachi, T. Imai, K. Watanabe, S. Toyokuni, M. Ueno, A.S. Zervos, G. Kroemer, T. Nakahata, A novel mechanism for imatinib mesylate-induced cell death of BCR-ABL-positive human leukemic cells: Caspase-independent, necrosis-like programmed cell death mediated by serine protease activity, *Blood* 103 (2004) 2299–2307.
- [61] Z. Chen, A.K. Tiwari, Multidrug resistance proteins (MRPs/ABCCs) in cancer chemotherapy and genetic diseases. *FEBS J.* 278 (2011) 3226–3245.

- [62] R.E. Pagano, C. Chen, Use of BODIPY-labeled sphingolipids to study membrane traffic along the endocytic pathway, *Ann. New York Acad. Sci.* 845 (1998) 152–160.
- [63] M. Kaneda, K. Takeuchi, K. Inoue, M. Umeda, Localization of the phosphatidylserine-binding site of glyceraldehyde-3-phosphate dehydrogenase responsible for membrane fusion. *J. Biochem.* 122 (1997) 1233–1240.
- [64] C.A.O. Stuermer, D.M. Lang, F. Kirsch, M. Wiechers, S. Deininger, H. Plattner, Glycosylphosphatidyl inositol-anchored proteins and fyn kinase assemble in noncaveolar plasma membrane microdomains defined by reggie-1 and -2. *Mol. Biol. Cell*, 12 (2001) 3031–3045.

**Table 1.** *In silico* physicochemical properties and drug-likeness of the *N*-pyrenyl derivatives (1–8)<sup>†</sup>

Compound No.	miLogP*	TPSA** (Å <sup>2</sup> )	Mol. wt.	No. of H-bond acceptor	No. of H-bond donor	No. of rotatable bond	Molecular Volume (Å <sup>3</sup> )	Drug-likeness Model Score
1	5.857	38.332	317.388	3	1	4	295.724	-0.14
2	5.755	21.261	303.405	2	1	5	293.542	-0.69
3	4.783	49.407	384.479	4	1	4	358.526	0.40
4	5.288	49.407	398.506	4	1	5	375.328	0.26
5	3.766	52.645	399.494	5	1	4	371.069	0.96
6	6.14	15.265	356.513	2	1	6	354.163	0.34
7	6.646	15.265	370.54	2	1	7	370.965	0.34
8	5.124	18.503	371.528	3	1	6	366.706	0.52

<sup>†</sup>Calculated by Molinspiration property engine v2013.09

\*lipophilicity

\*\*total polar surface area

**Table 2.** *In silico* predicted bioactivity of the *N*-pyrenyl derivatives (1–8)<sup>‡</sup>

Compound No.	GPCR ligand	Ion channel modulator	Kinase inhibitor	Nuclear receptor ligand	Protease inhibitor	Enzyme inhibitor
1	0.16	0.20	0.09	0.12	0.25	0.11
2	0.02	0.01	0.03	-0.07	0.04	-0.06
3	0.10	0.01	0.01	-0.16	0.09	0.00
4	0.09	0.01	0.01	-0.15	0.08	0.00
5	0.10	0.03	0.06	-0.20	0.06	-0.01
6	0.20	0.18	0.19	-0.00	0.11	0.11
7	0.19	0.17	0.18	-0.00	0.10	0.11
8	0.24	0.21	0.26	-0.05	0.10	0.11

<sup>‡</sup>Calculated by Molinspiration bioactivity score v2011.06

**Table 3.** IC<sub>50</sub> values (μM) of pyrenyl derivatives against a panel of cancer cell lines

Compounds	Cells	HepG2	Hepa1-6	HT-29	HeLa	MCF7	Caco-2
<b>1</b>		30.4±5.0 <sup>†</sup>	5.9±2.5 <sup>†</sup>	20.7±3.8 <sup>†</sup>	16.2±3.8 <sup>†</sup>	ND	36.3±3.6 <sup>†</sup>
<b>2</b>		39.6±7.1 <sup>†</sup>	9.9±5.2 <sup>†</sup>	14.0±5.7 <sup>†</sup>	9.8±1.03 <sup>†</sup>	ND	>50 <sup>†</sup>
<b>3</b>		>30	>30	ND	>30	ND	ND
<b>4</b>		ND	>30	>30	>30	>30	ND
<b>5</b>		16.9±3.6	14.8*	19.3±5.5	16.8*	14.1*	ND
<b>6</b>		1.4±0.2	2.5±1.4	2.98*	2.6±1.2	1.1±0.01	ND
<b>7</b>		18.8±2.9	18.3±1.4	19.8*	18.2±1.4	14.1±0.9	ND
<b>8</b>		2.4±1.5	1.1±0.2	4.8±0.1	4.1±1.2	2.6±0.6	7.2266*

<sup>†</sup> See reference [15]

\* Based on single dose curve

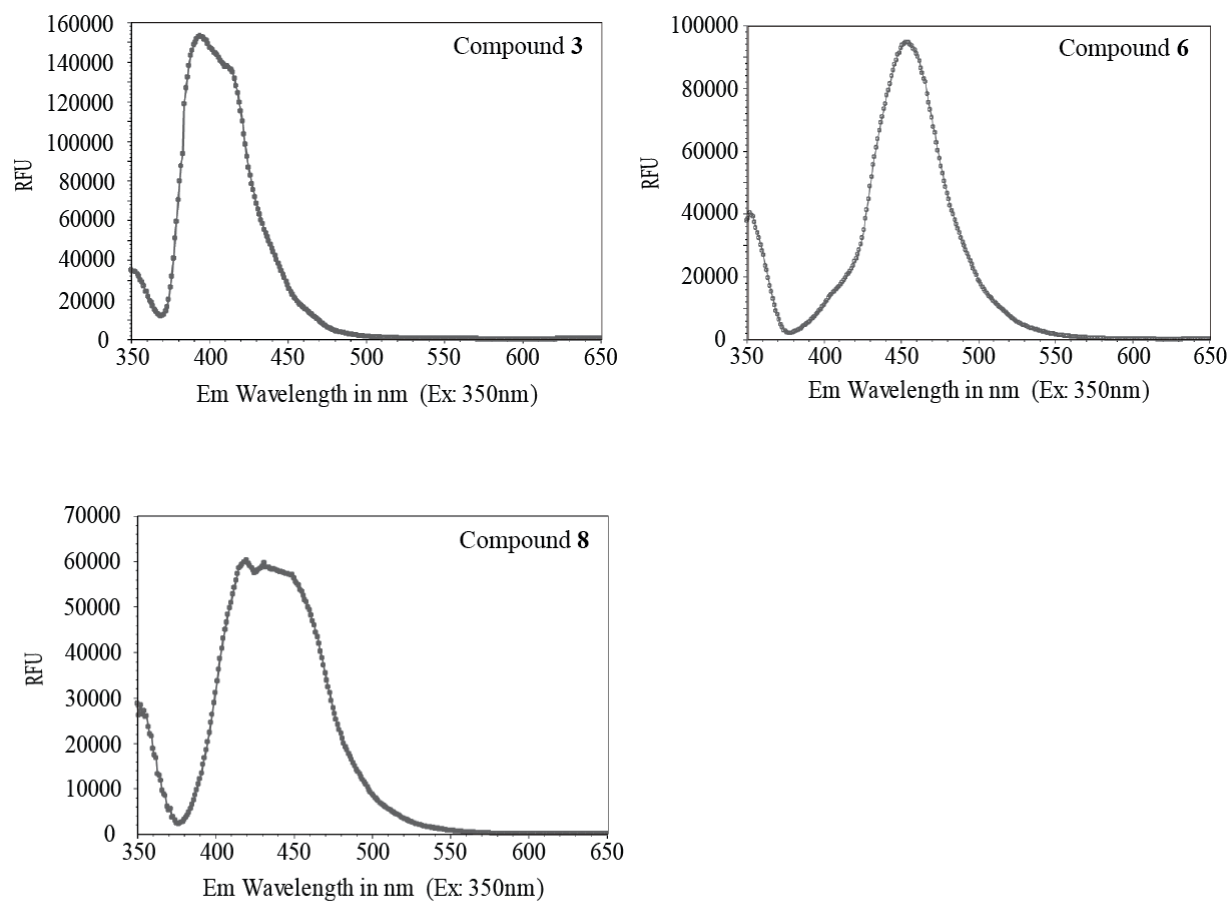


**Figure 1.** Spectral emission analysis of novel pyrenyl derivatives (**3**, **6**, and **8**). The fluorescence emission spectra of the indicated compound (50  $\mu$ M) between the wavelengths of 350-650 nm, as measured in relative fluorescent units (RFUs), was determined upon excitation at 350 nm.

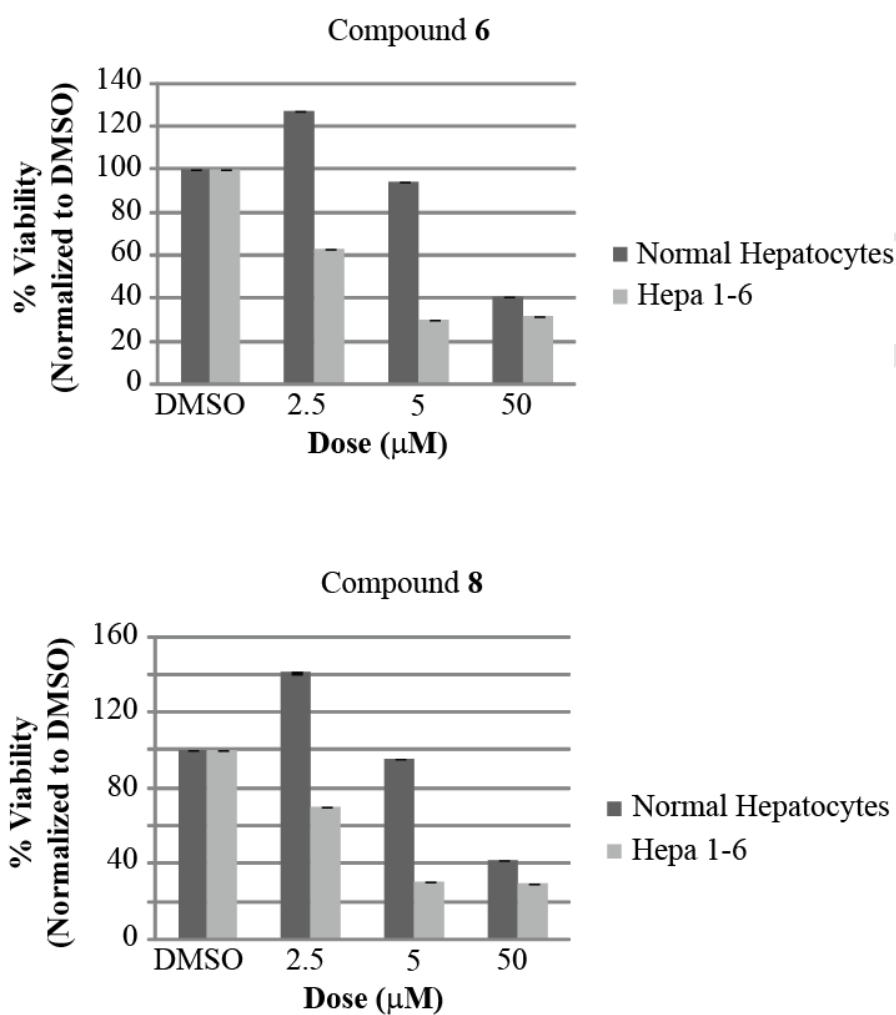


**Figure 2.** Selective cytotoxicity of novel pyrenyl compounds. The cell viability of primary mouse hepatocytes or Hepa 1-6 cancer cells was analyzed after cells were treated with the indicated doses of compound **6** (A) or compound **8** (B) for 48 hrs. For each cell type, viability was normalized to DMSO-treated cells.

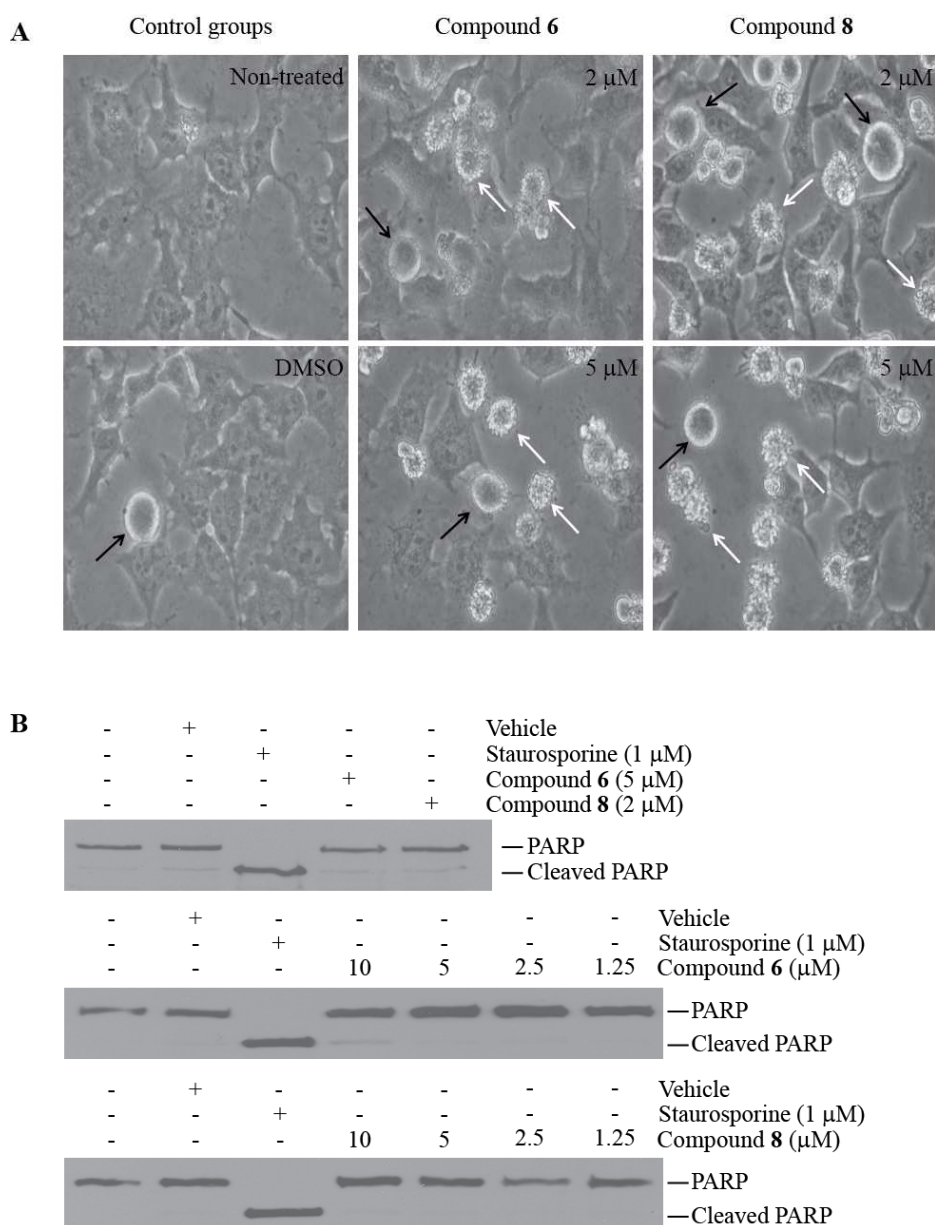


**Figure 3.** Cytotoxic pyrenyl derivatives cause membrane blebbing without inducing PARP cleavage. (A) HeLa cells, which were treated with the indicated dose of either compound **6** or **8**, were analyzed microscopically for changes in membrane morphology. Cells exhibiting cell shrinkage along with membrane blebbing are indicated with white arrows, whereas cells exhibiting an enlarged and rounded appearance are indicated with dark arrows. (B) Lysates from HeLa cells that were treated with the indicated dose of either compound **6** or **8** were analyzed by western blotting for PARP as well as cleaved PARP. Staurosporine (1  $\mu$ M) was used as a positive control for PARP cleavage.

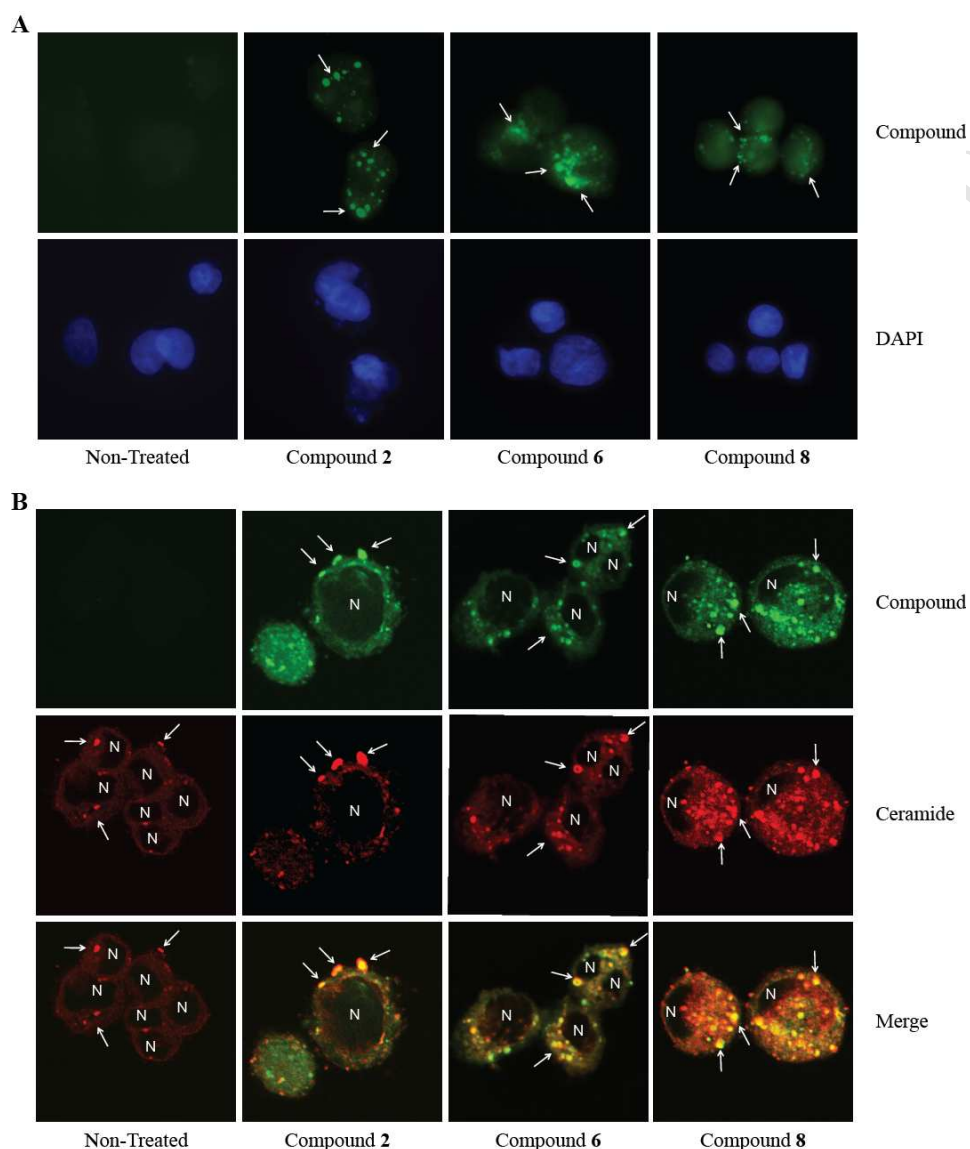


**Figure 4.** Novel pyrenyl derivatives co-localize with ceramide at cell membrane. (A) HepG2 cells, which were treated with the indicated compound, were analyzed by epifluorescent microscopy. Cells were also labeled with DAPI for nuclear staining. Punctate pattern for each compound in the cellular membrane is indicated with white arrows. (B) HepG2 cells were treated with the indicated compound along with BODIPY-TR-conjugated ceramide analogs and examined by confocal epifluorescent microscopy. Co-localization of the pyrenyl compounds with ceramide is indicated by white arrows and appears as yellow punctate structures in the merged image (bottom panels). Nuclei, which lack either compound or ceramide, are labeled with 'N'.

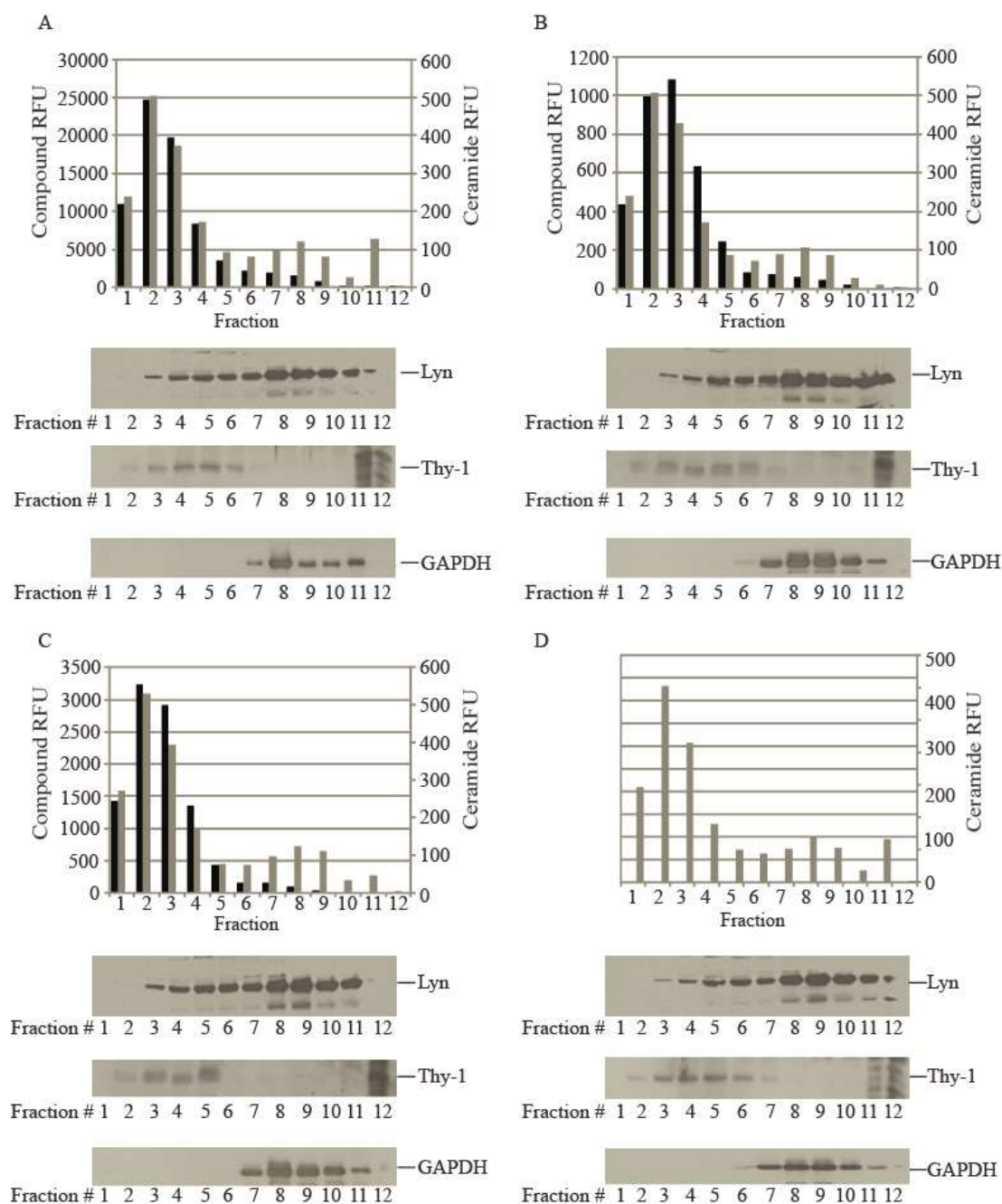


**Figure 5.** Pyrenyl derivatives partially overlap with lipophilic molecules in biochemical fractionation of HepG2 cells. Lysates from HepG2 cells that were treated with compound **2** (A), compound **6** (B), compound **8** (C), or vehicle control (D) along with BODIPY TR-labeled ceramide analogs were fractionated on a step-wise OptiPrep<sup>TM</sup> density gradient. Fractions were then analyzed for the fluorescence emission of pyrenyl compounds (black bars; left y-axis) or ceramide (gray bars; right y-axis), each of which was measured in relative fluorescence units (RFUs). Fractions were also analyzed for the presence of the Lyn kinase (top panels), Thy-1 (middle panels), or GAPDH (bottom panels) by western blotting.

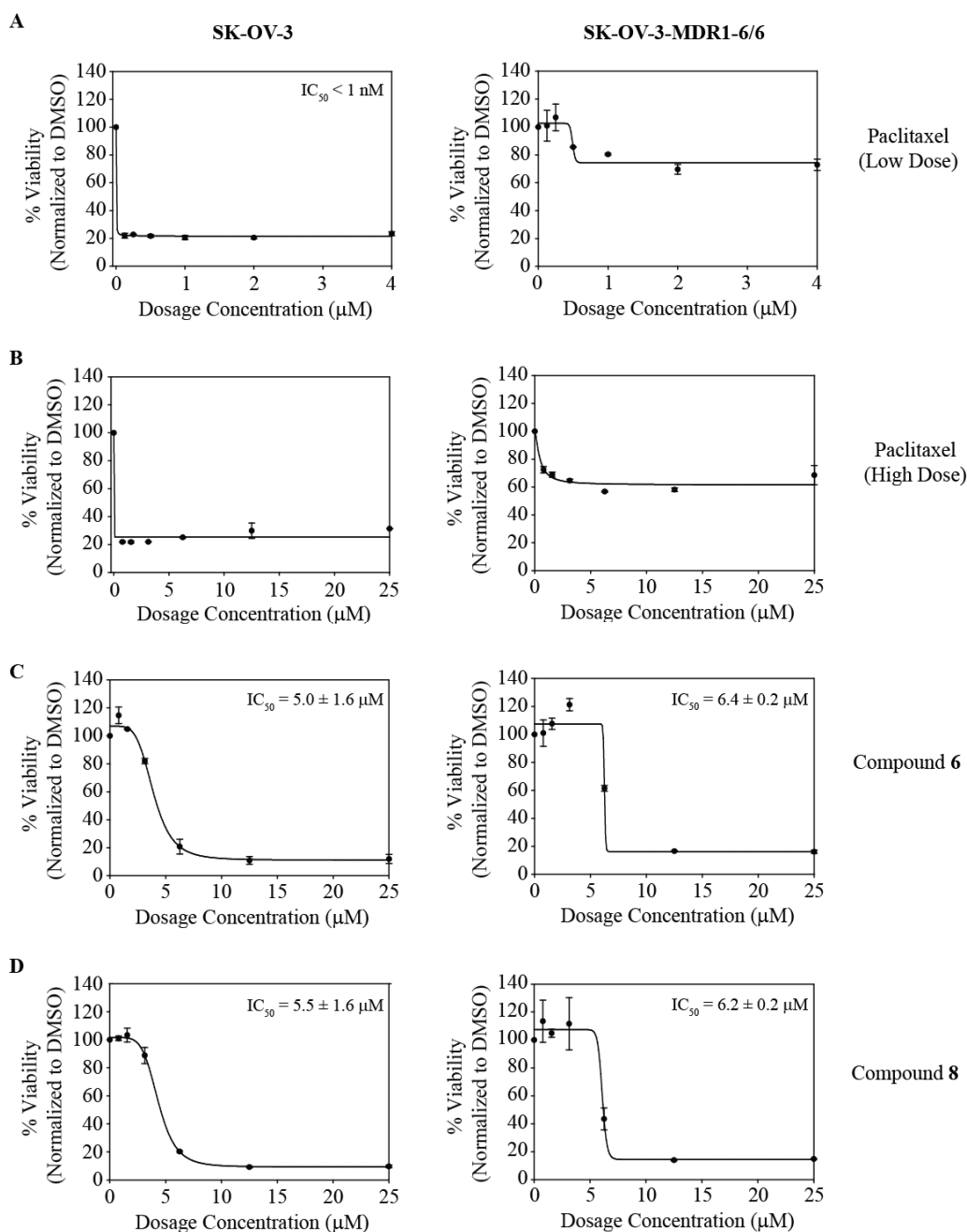


**Figure 6.** Cytotoxic pyrenyl derivatives circumvent MDR1-mediated drug resistance *in vitro*. SKOV3 cells (left panels) or SKOV3-MDR1-M6/6 cells (right panels) were treated with increasing concentrations of Paclitaxel at low (A) and high dosages (B), compound **6** (C), or compound **8** (D) for 48 hrs. Cell viability was then analyzed using a SRB assay, and the dose curve for each compound in each cell line was plotted. The calculated  $IC_{50}$  value for each compound is indicated in the top right corner of each graph. A representative experiment is shown ( $n \geq 2$ ).

**Table 1.** *In silico* physicochemical properties and drug-likeness of the *N*-pyrenyl derivatives (1–8)<sup>†</sup>

Compound No.	miLogP*	TPSA** (Å <sup>2</sup> )	Mol. wt.	No. of H-bond acceptor	No. of H-bond donor	No. of rotatable bond	Molecular Volume (Å <sup>3</sup> )	Drug-likeness Model Score
<b>1</b>	5.857	38.332	317.388	3	1	4	295.724	-0.14
<b>2</b>	5.755	21.261	303.405	2	1	5	293.542	-0.69
<b>3</b>	4.783	49.407	384.479	4	1	4	358.526	0.40
<b>4</b>	5.288	49.407	398.506	4	1	5	375.328	0.26
<b>5</b>	3.766	52.645	399.494	5	1	4	371.069	0.96
<b>6</b>	6.14	15.265	356.513	2	1	6	354.163	0.34
<b>7</b>	6.646	15.265	370.54	2	1	7	370.965	0.34
<b>8</b>	5.124	18.503	371.528	3	1	6	366.706	0.52

<sup>†</sup>Calculated by Molinspiration property engine v2013.09

\*lipophilicity

\*\*total polar surface area

**Table 2.** *In silico* predicted bioactivity of the *N*-pyrenyl derivatives (**1–8**)<sup>‡</sup>

Compound No.	GPCR ligand	Ion channel modulator	Kinase inhibitor	Nuclear receptor ligand	Protease inhibitor	Enzyme inhibitor
<b>1</b>	0.16	0.20	0.09	0.12	0.25	0.11
<b>2</b>	0.02	0.01	0.03	-0.07	0.04	-0.06
<b>3</b>	0.10	0.01	0.01	-0.16	0.09	0.00
<b>4</b>	0.09	0.01	0.01	-0.15	0.08	0.00
<b>5</b>	0.10	0.03	0.06	-0.20	0.06	-0.01
<b>6</b>	0.20	0.18	0.19	-0.00	0.11	0.11
<b>7</b>	0.19	0.17	0.18	-0.00	0.10	0.11
<b>8</b>	0.24	0.21	0.26	-0.05	0.10	0.11

<sup>‡</sup>Calculated by Molinspiration bioactivity score v2011.06

**Table 3.** IC<sub>50</sub> values (μM) of pyrenyl derivatives against a panel of cancer cell lines

Compounds	Cells	HepG2	Hepa1-6	HT-29	HeLa	MCF7	Caco-2
<b>1</b>		30.4±5.0 <sup>†</sup>	5.9±2.5 <sup>†</sup>	20.7±3.8 <sup>†</sup>	16.2±3.8 <sup>†</sup>	ND	36.3±3.6 <sup>†</sup>
<b>2</b>		39.6±7.1 <sup>†</sup>	9.9±5.2 <sup>†</sup>	14.0±5.7 <sup>†</sup>	9.8±1.03 <sup>†</sup>	ND	>50 <sup>†</sup>
<b>3</b>		>30	>30	ND	>30	ND	ND
<b>4</b>		ND	>30	>30	>30	>30	ND
<b>5</b>		16.9±3.6	14.8*	19.3±5.5	16.8*	14.1*	ND
<b>6</b>		1.4±0.2	2.5±1.4	2.98*	2.6±1.2	1.1±0.01	ND
<b>7</b>		18.8±2.9	18.3±1.4	19.8*	18.2±1.4	14.1±0.9	ND
<b>8</b>		2.4±1.5	1.1±0.2	4.8±0.1	4.1±1.2	2.6±0.6	7.2266*

<sup>†</sup> See reference [15]

\* Based on single dose curve

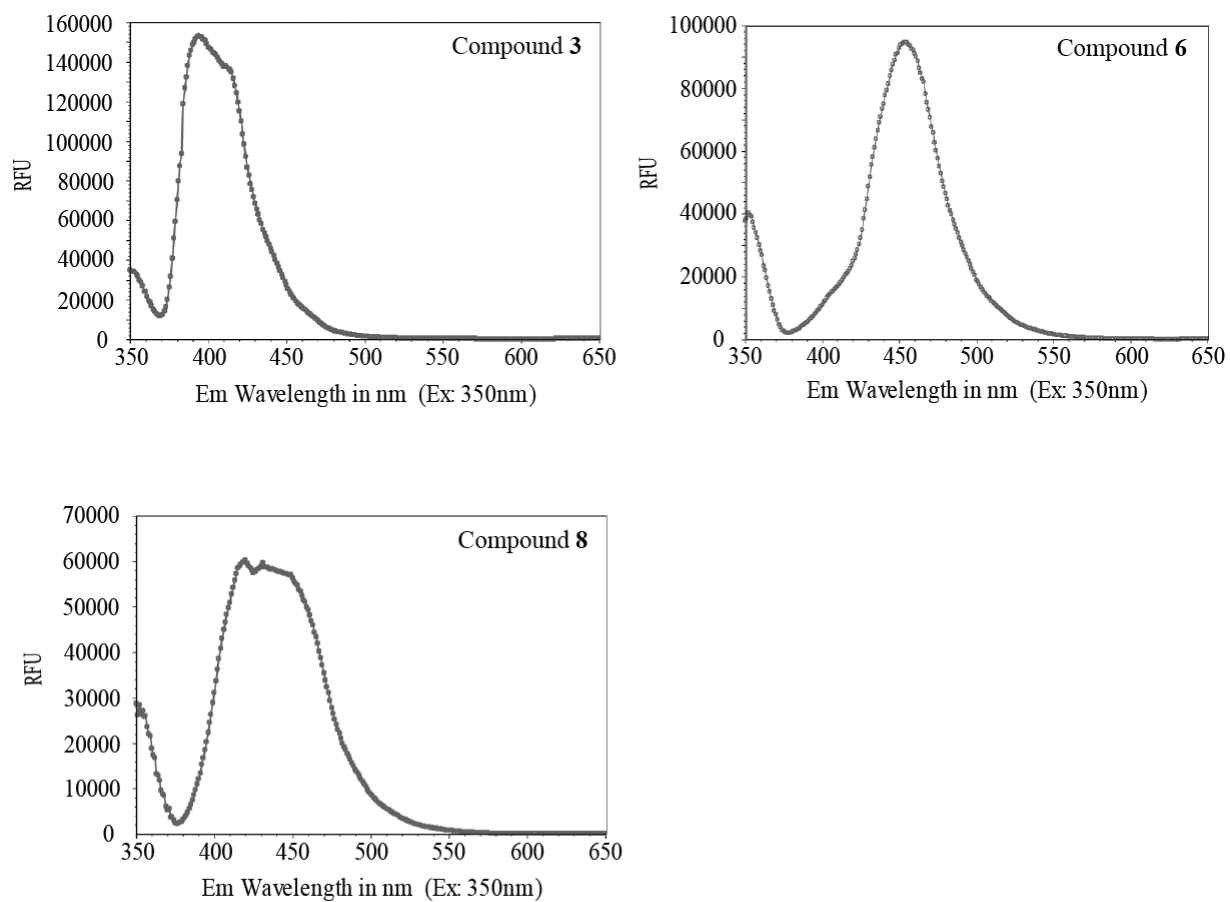


**Figure 1.** Spectral emission analysis of novel pyrenyl derivatives (**3**, **6**, and **8**). The fluorescence emission spectra of the indicated compound (50  $\mu$ M) between the wavelengths of 350-650 nm, as measured in relative fluorescent units (RFUs), was determined upon excitation at 350 nm.

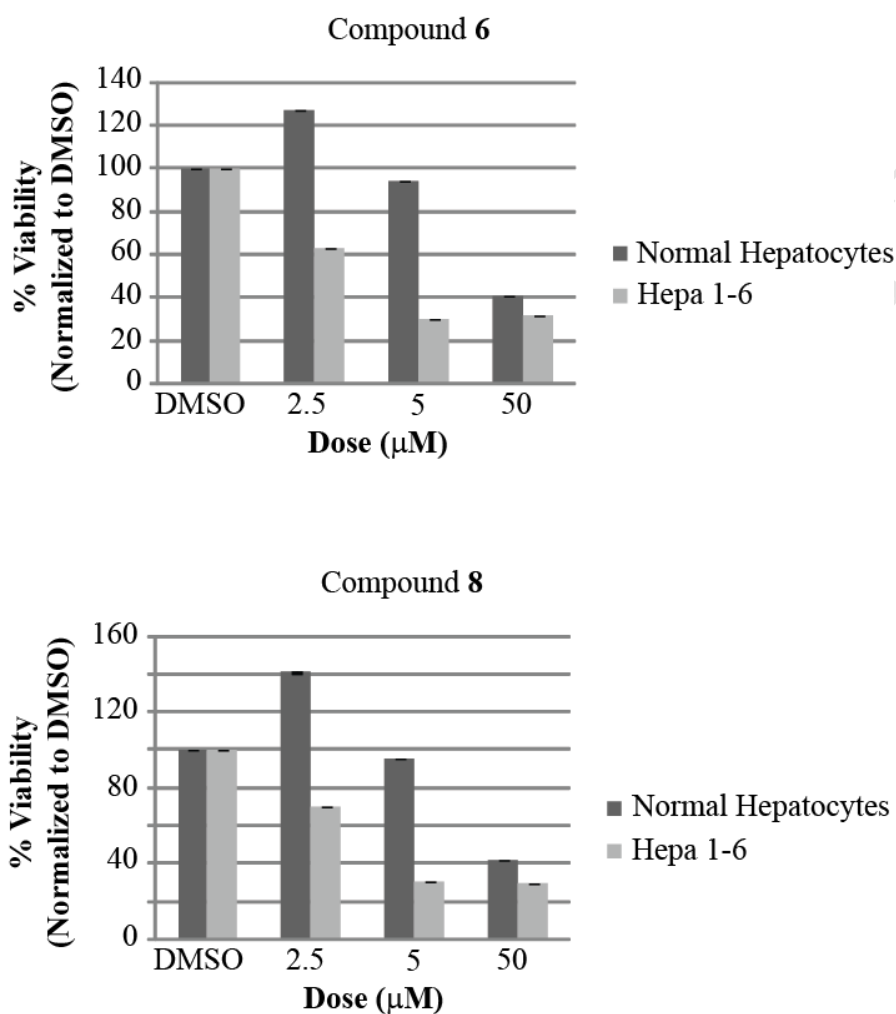


**Figure 2.** Selective cytotoxicity of novel pyrenyl compounds. The cell viability of primary mouse hepatocytes or Hepa 1-6 cancer cells was analyzed after cells were treated with the indicated doses of compound **6** (A) or compound **8** (B) for 48 hrs. For each cell type, viability was normalized to DMSO-treated cells.

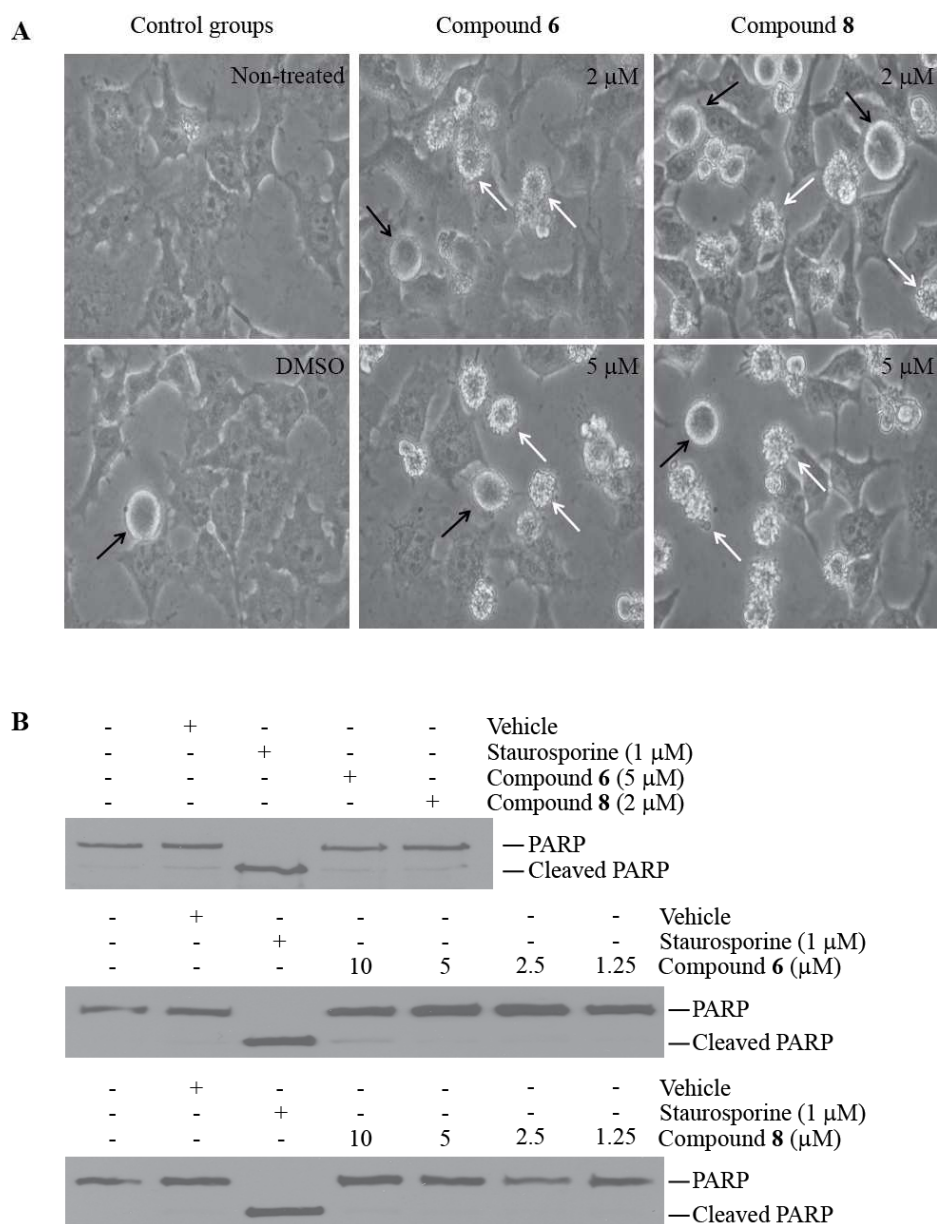


**Figure 3.** Cytotoxic pyrenyl derivatives cause membrane blebbing without inducing PARP cleavage. (A) HeLa cells, which were treated with the indicated dose of either compound **6** or **8**, were analyzed microscopically for changes in membrane morphology. Cells exhibiting cell shrinkage along with membrane blebbing are indicated with white arrows, whereas cells exhibiting an enlarged and rounded appearance are indicated with dark arrows. (B) Lysates from HeLa cells that were treated with the indicated dose of either compound **6** or **8** were analyzed by western blotting for PARP as well as cleaved PARP. Staurosporine (1  $\mu$ M) was used as a positive control for PARP cleavage.

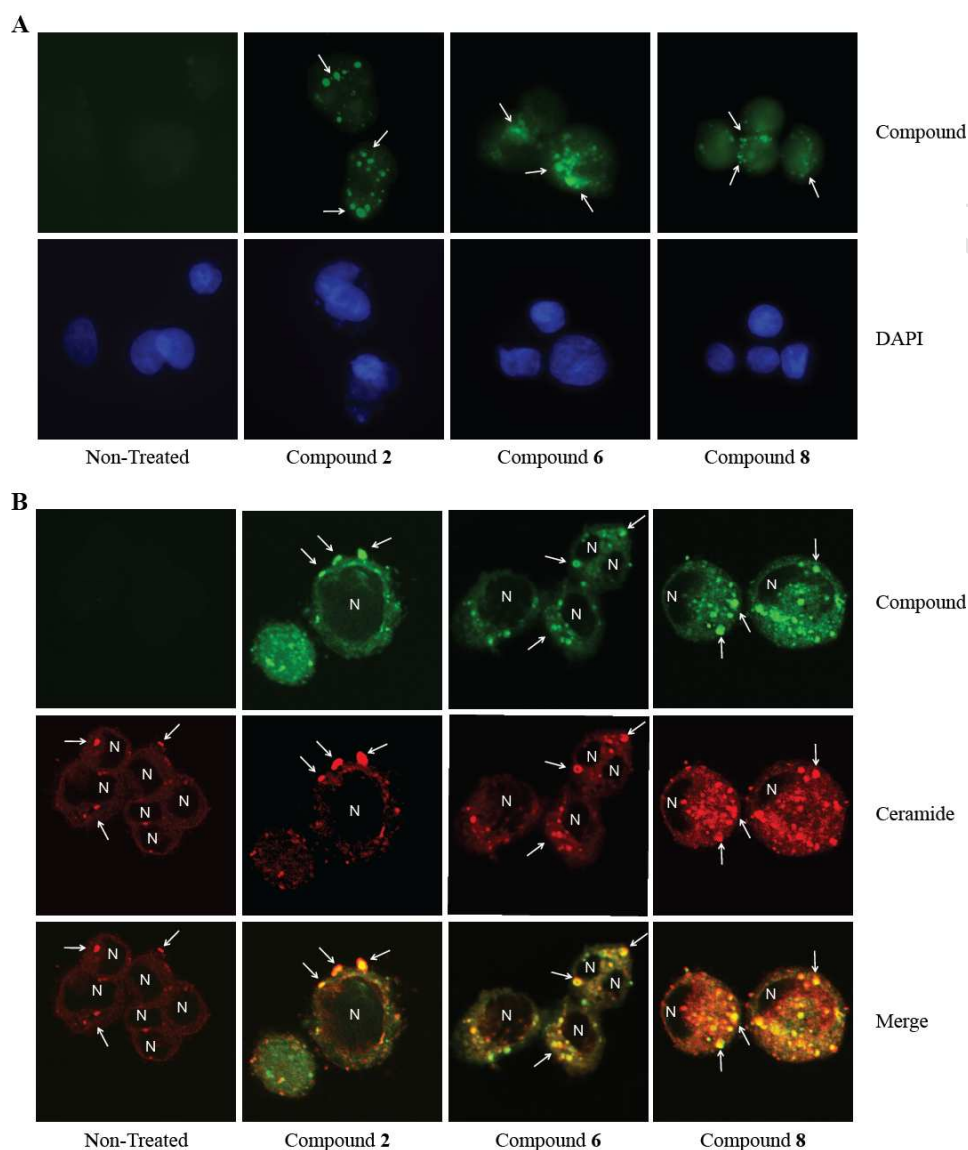


**Figure 4.** Novel pyrenyl derivatives co-localize with ceramide at cell membrane. (A) HepG2 cells, which were treated with the indicated compound, were analyzed by epifluorescent microscopy. Cells were also labeled with DAPI for nuclear staining. Punctate pattern for each compound in the cellular membrane is indicated with white arrows. (B) HepG2 cells were treated with the indicated compound along with BODIPY-TR-conjugated ceramide analogs and examined by confocal epifluorescent microscopy. Co-localization of the pyrenyl compounds with ceramide is indicated by white arrows and appears as yellow punctate structures in the merged image (bottom panels). Nuclei, which lack either compound or ceramide, are labeled with 'N'.

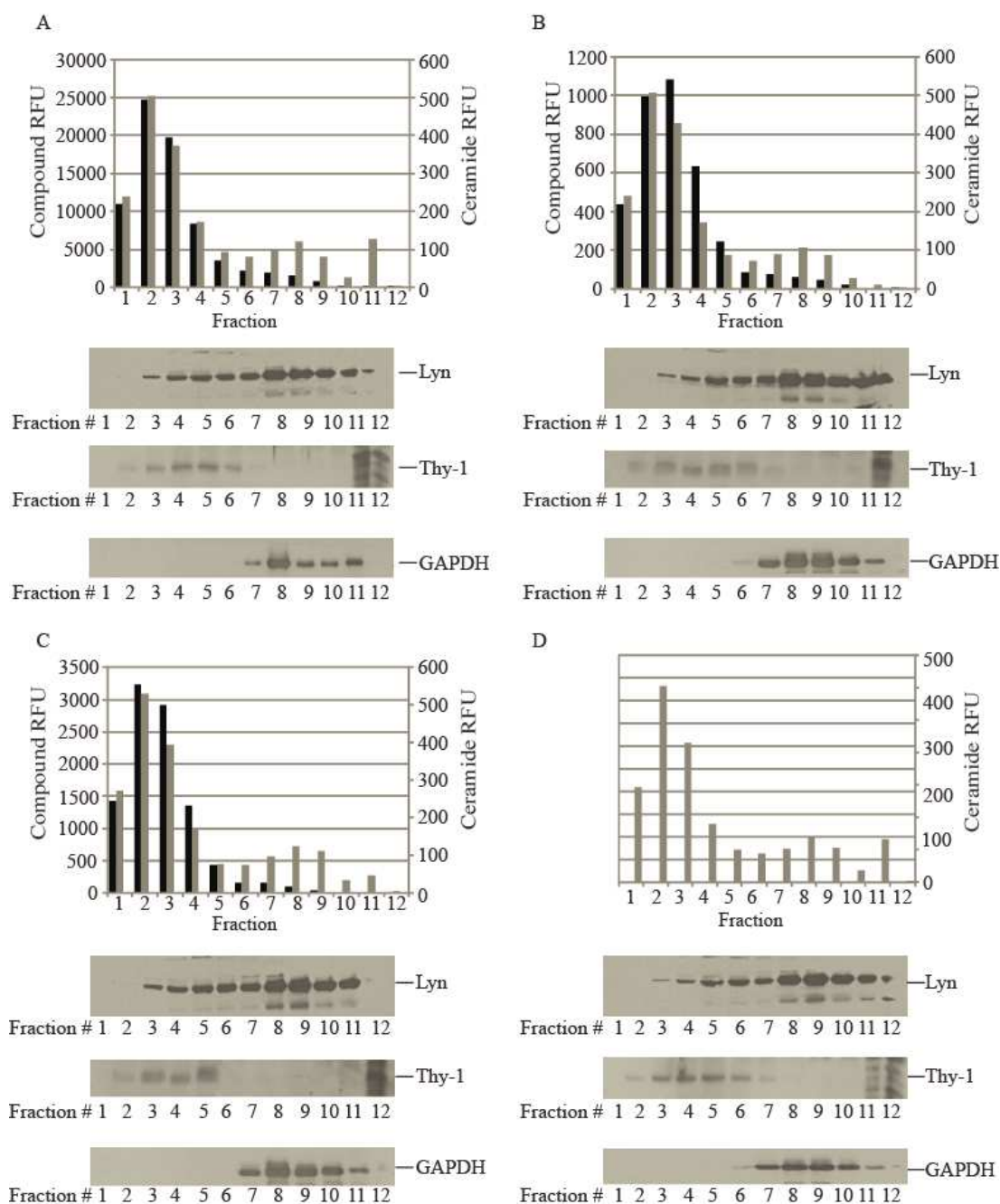


**Figure 5.** Pyrenyl derivatives partially overlap with lipophilic molecules in biochemical fractionation of HepG2 cells. Lysates from HepG2 cells that were treated with compound **2** (A), compound **6** (B), compound **8** (C), or vehicle control (D) along with BODIPY TR-labeled ceramide analogs were fractionated on a step-wise OptiPrep™ density gradient. Fractions were then analyzed for the fluorescence emission of pyrenyl compounds (black bars; left y-axis) or ceramide (gray bars; right y-axis), each of which was measured in relative fluorescence units (RFUs). Fractions were also analyzed for the presence of the Lyn kinase (top panels), Thy-1 (middle panels), or GAPDH (bottom panels) by western blotting.

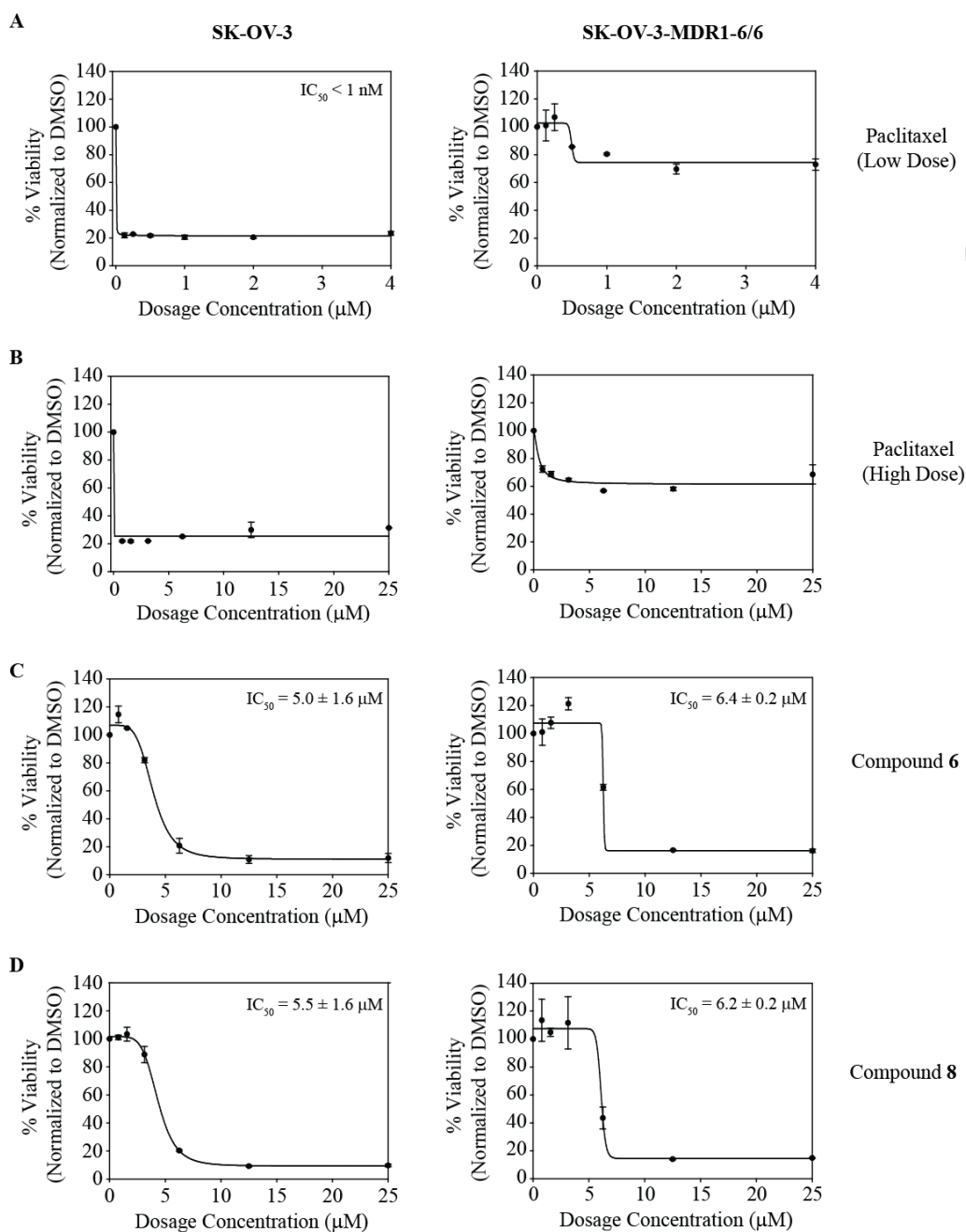
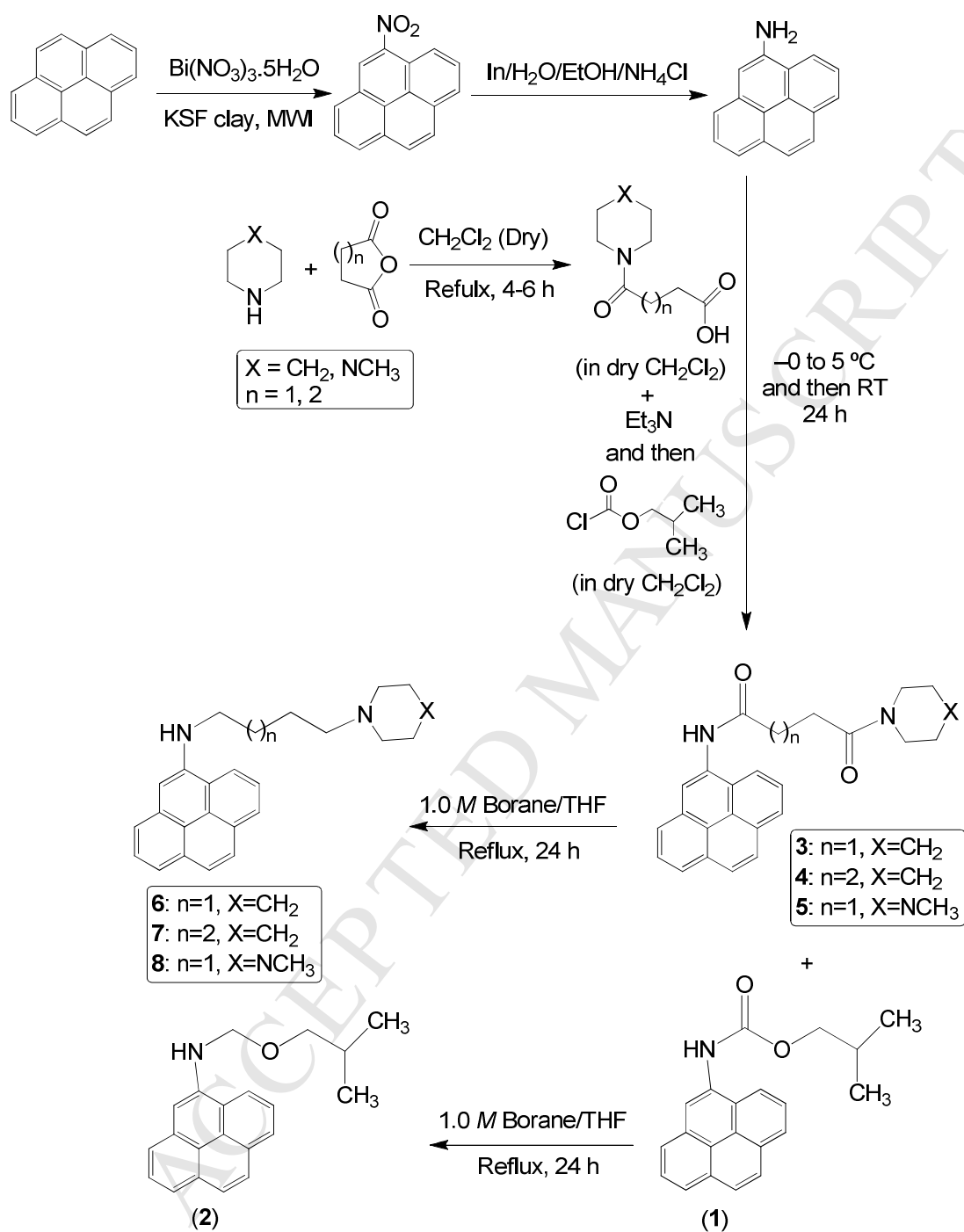


**Figure 6.** Cytotoxic pyrenyl derivatives circumvent MDR1-mediated drug resistance *in vitro*. SKOV3 cells (left panels) or SKOV3-MDR1-M6/6 cells (right panels) were treated with increasing concentrations of Paclitaxel at low (A) and high dosages (B), compound 6 (C), or compound 8 (D) for 48 hrs. Cell viability was then analyzed using a SRB assay, and the dose curve for each compound in each cell line was plotted. The calculated  $IC_{50}$  value for each compound is indicated in the top right corner of each graph. A representative experiment is shown ( $n \geq 2$ ).



Scheme 1: Synthesis of the pyrenyl derivatives (1-8)

**Research highlights (EJMECH-D-14-01470)****Design, synthesis and biological evaluation of novel pyrenyl derivatives as anticancer agents**

Debasish Bandyopadhyay, Jorge L. Sanchez, Adrian M. Guerrero, Fang-Mei Chang, Jose C. Granados, John D. Short, and Bimal K. Banik

- ❖ A series of pyrene derivatives have been synthesized following multi-step process.
- ❖ Virtual screening for druggability of the *N*-pyrenyl derivatives **1–8** is reported.
- ❖ Four-carbon linker diamines are selectively cytotoxic for a series of cancer cells.
- ❖ The cytotoxicity occurs in a caspase-independent manner.
- ❖ Compounds **6** & **8** circumvented P-gp mediated drug resistance in ovarian cancer cells.

## Supporting Information

for

### Design, synthesis and biological evaluation of novel pyrenyl derivatives as anticancer agents

**Debasish Bandyopadhyay<sup>1</sup>, Jorge L. Sanchez<sup>1,2</sup>, Adrian M. Guerrero<sup>1</sup>, Fang-Mei Chang<sup>2</sup>, Jose C. Granados<sup>2</sup>, John D. Short<sup>2,3,\*</sup>, and Bimal K. Banik<sup>1,\*</sup>**

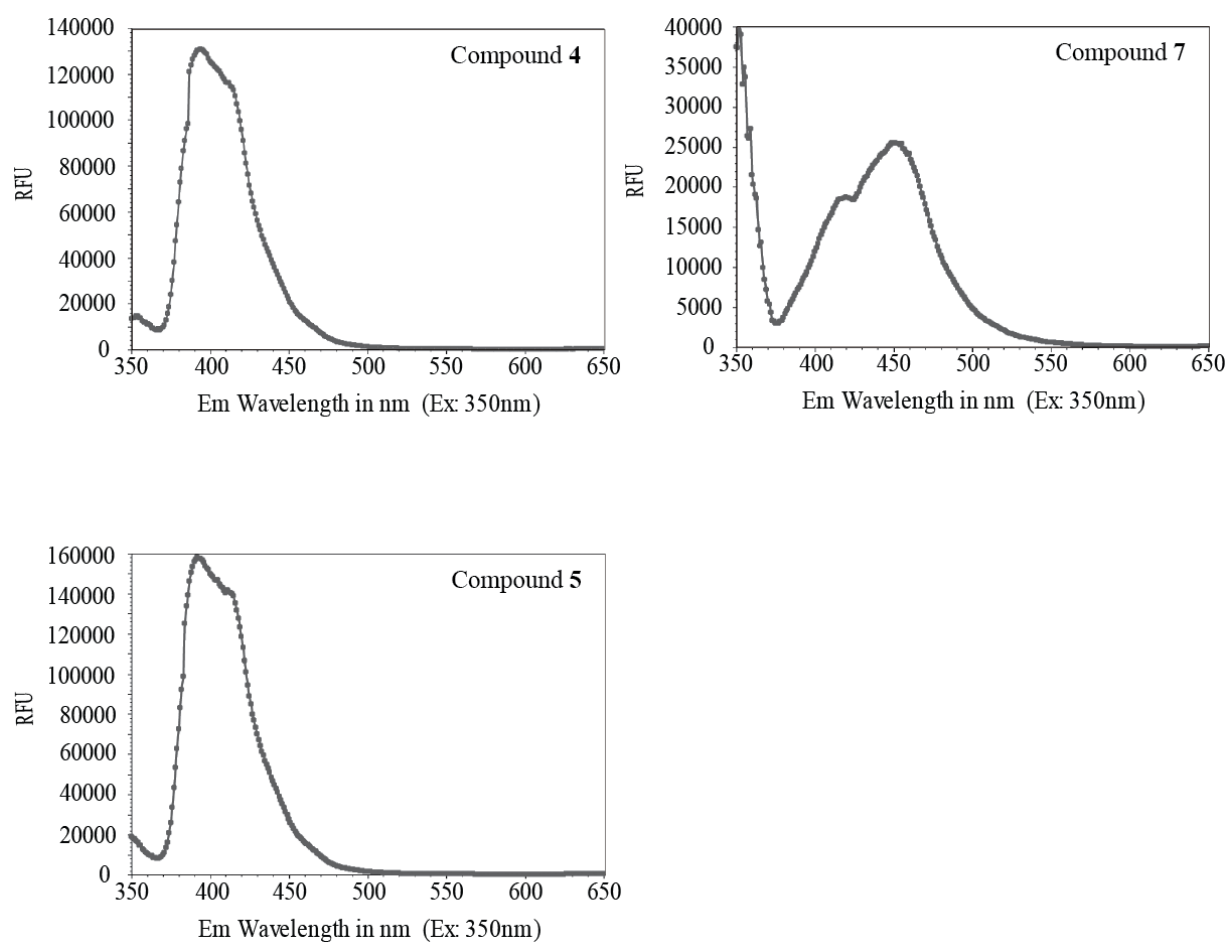
<sup>1</sup>Department of Chemistry, The University of Texas-Pan American, 1201 West University Drive, Edinburg, Texas 78539, USA

<sup>2</sup>University of Texas Health Science Center at San Antonio-Regional Academic Health Center, Medical Research Division, 1214 West Schunior Street, Edinburg, TX 78541, USA

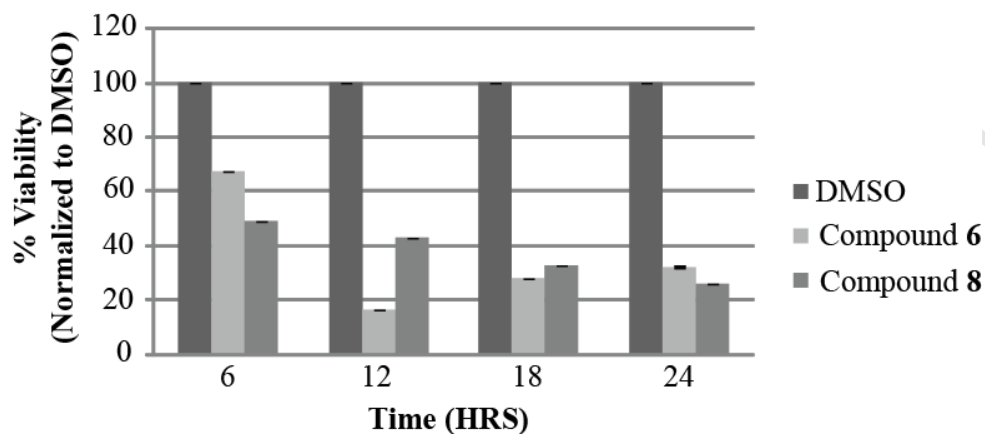
<sup>3</sup>Department of Pharmacology, University of Texas Health Science Center at San Antonio, 7703 Floyd Curl Drive, San Antonio, TX 78229, USA

\*Corresponding authors, Ph: +1(956)6658741, Fax: +1(956)3845006, E-mails: [bandyopad@utpa.edu](mailto:bandyopad@utpa.edu) or [shortj@uthscsa.edu](mailto:shortj@uthscsa.edu)

The following information can be found online: (1) The fluorescence emission spectra of three compounds (**4**, **5**, and **7**), (2) the time-course for compounds **6** and **8** causing cytotoxicity of HepG2 cells, and (3) the infrared (IR), proton magnetic resonance (PMR) and carbon magnetic resonance (CMR) spectra of compounds **3–8** can be found as in the sequel.

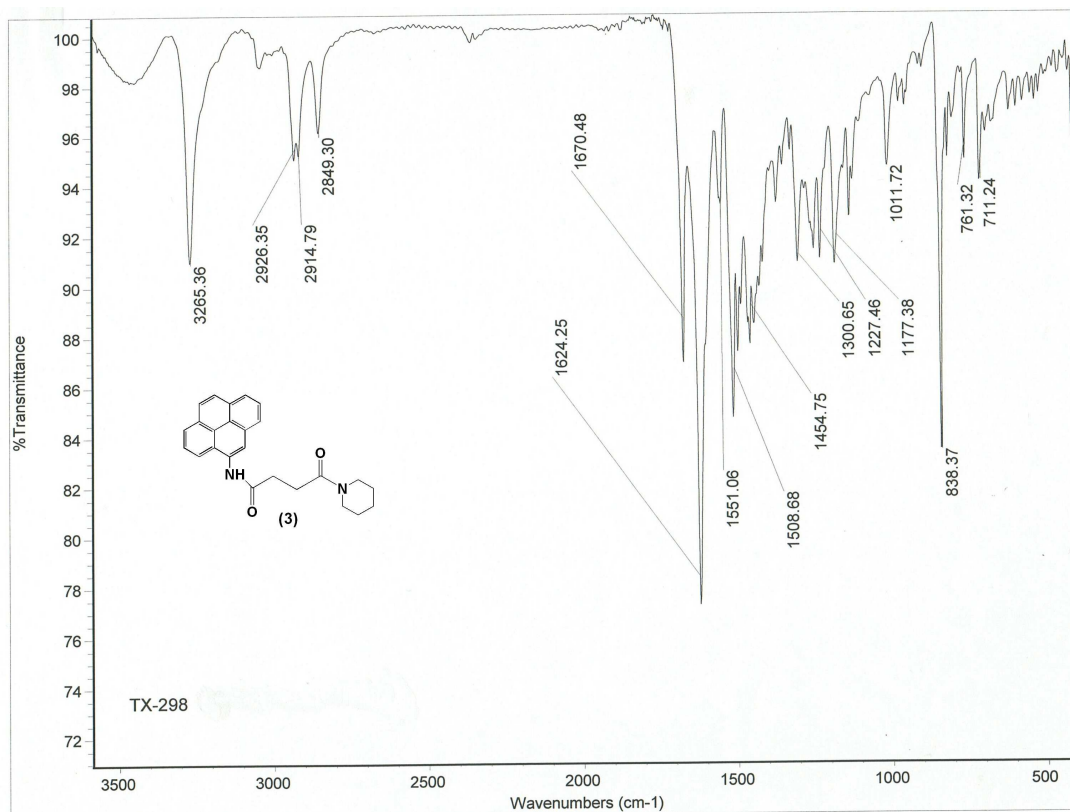


**Supplemental Figure 1.** Spectral emission analysis of novel pyrenyl derivatives (**4**, **5**, and **7**). The fluorescence emission spectra of the indicated compound (50  $\mu$ M) between the wavelengths of 350-650 nm, as measured in relative fluorescent units (RFUs), was determined upon excitation at 350 nm.



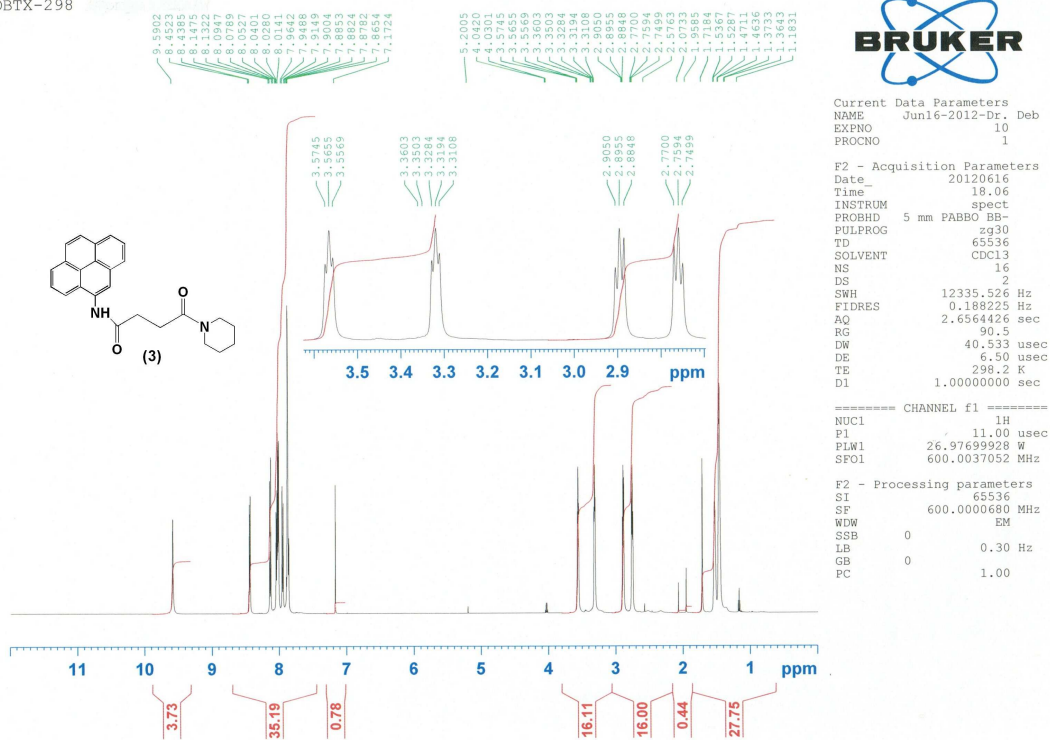
**Supplemental Figure 2:** Time-course for compounds **6** and **8** against HepG2 cells.

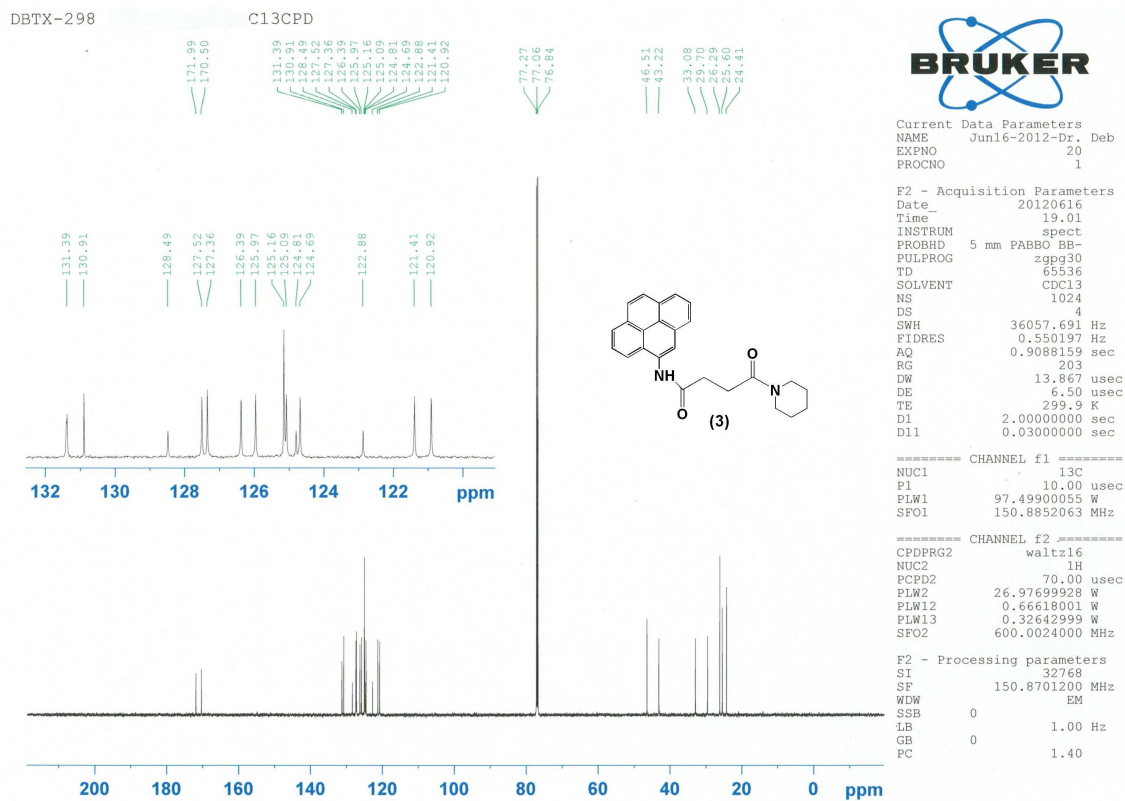
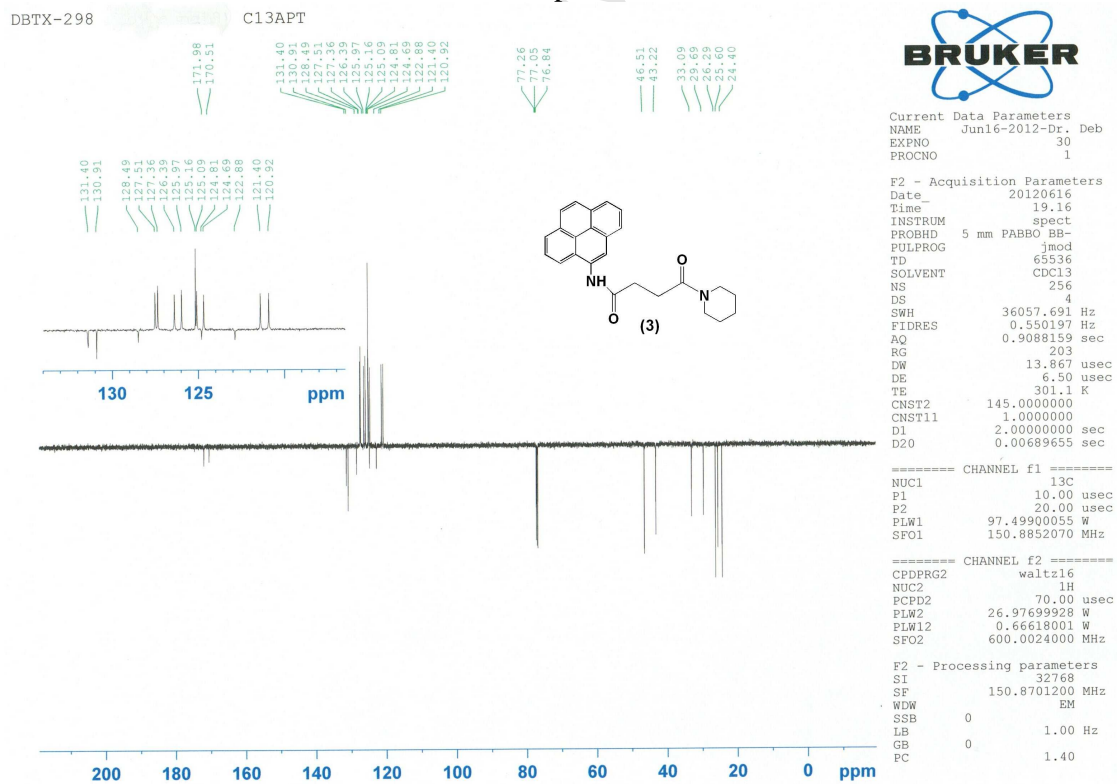
Each data point represents the mean  $\pm$  standard deviation value, and a representative experiment is shown. These data indicate that **6** and **8**, when used at 5  $\mu$ M, cause cell death between 6 and 12 hrs of cellular exposure, reducing cell viability greater than 70%.

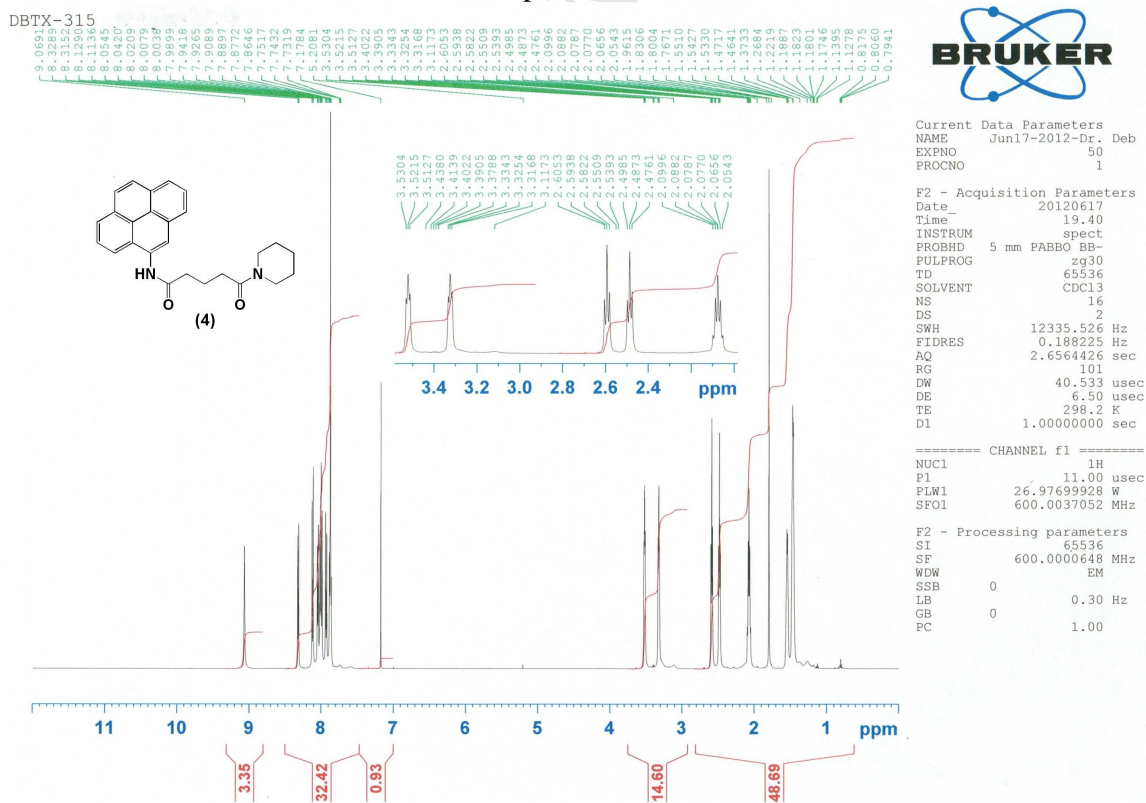
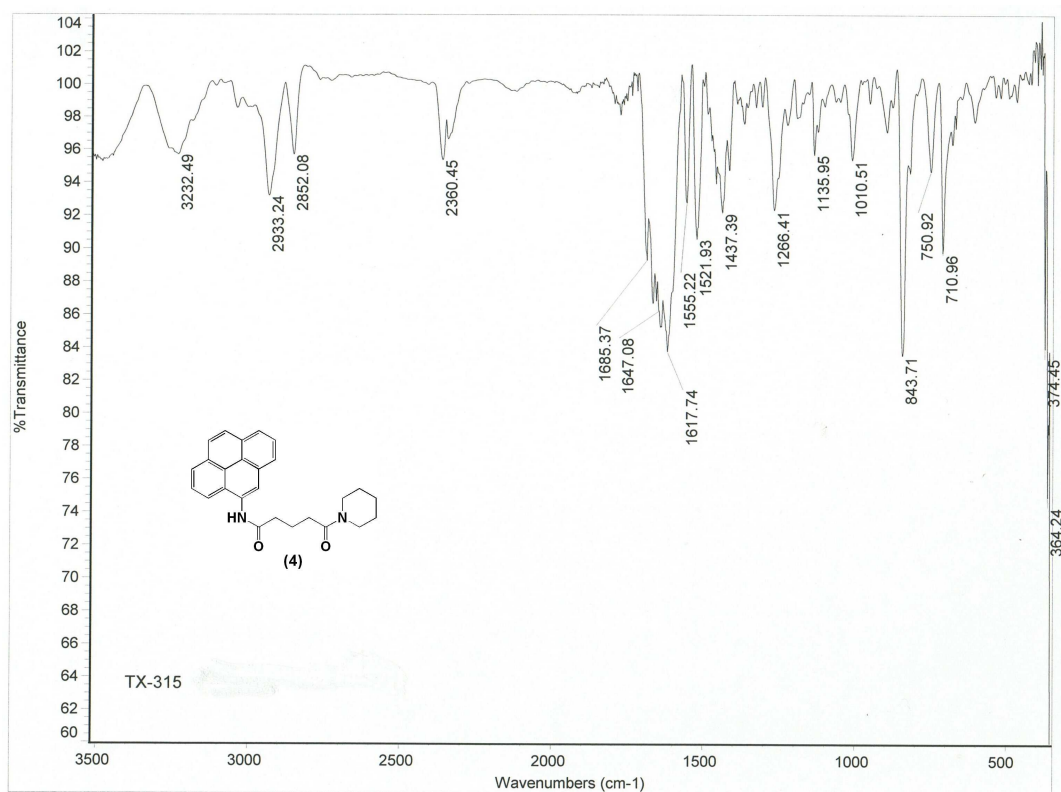


IR Spectrum of 3

DBTX-298

<sup>1</sup>H-NMR Spectrum of 3

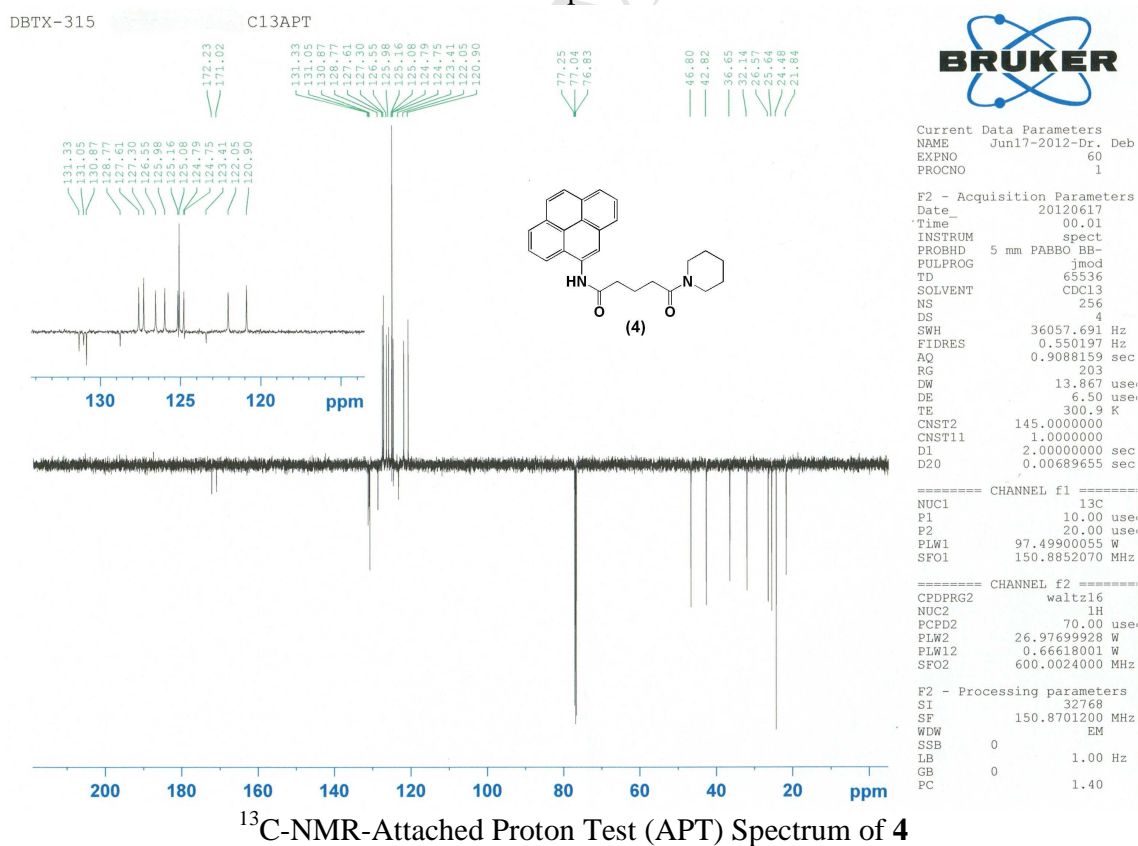
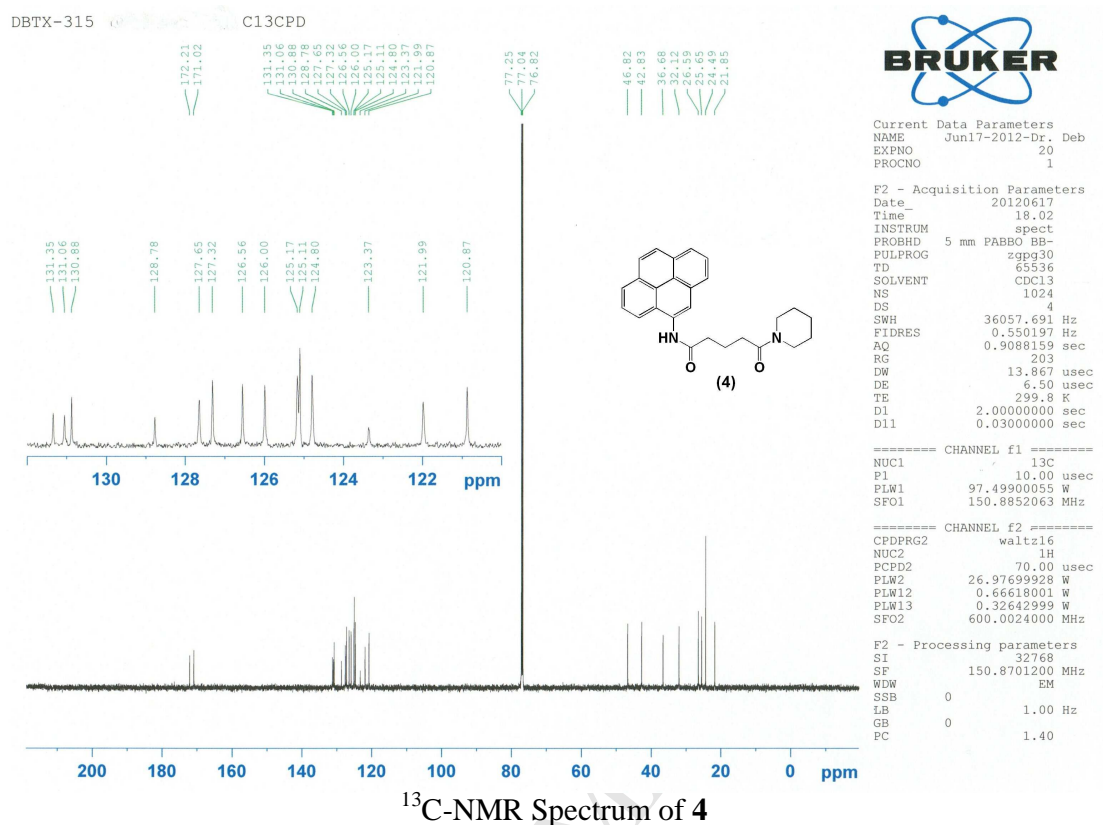
 $^{13}\text{C}$ -NMR Spectrum of **3** $^{13}\text{C}$ -NMR-Attached Proton Test (APT) Spectrum of **3**

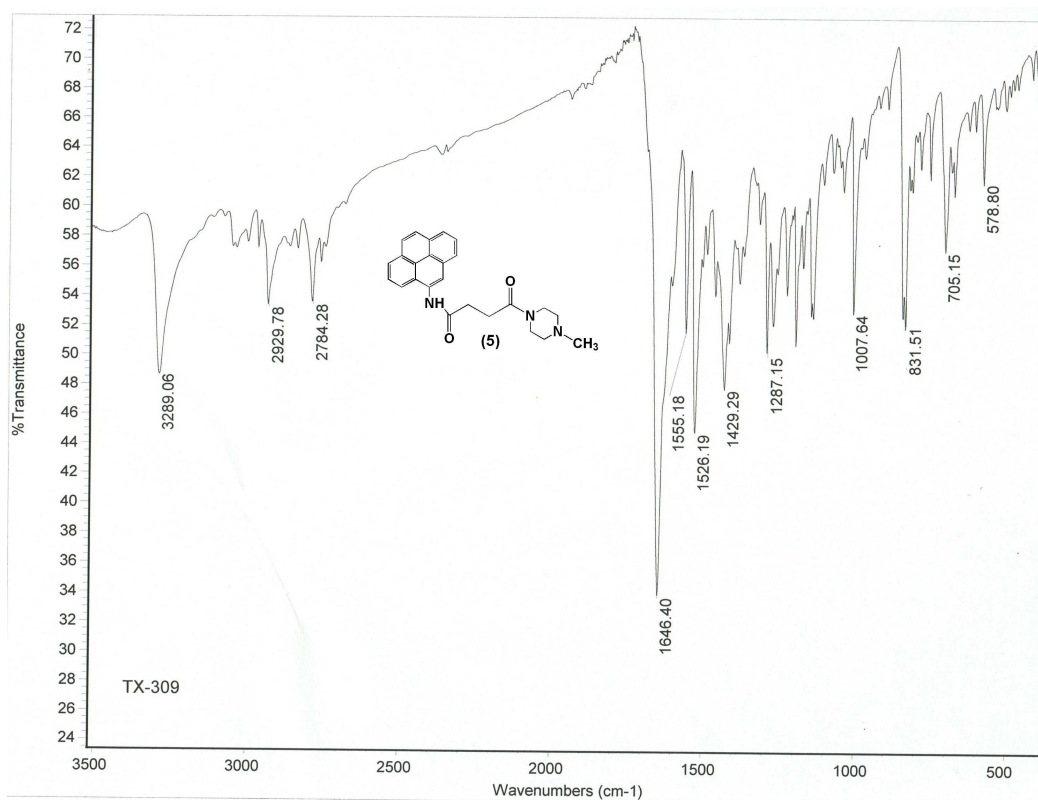


Current Data Parameters  
 NAME Jun17-2012-Dr. Deb  
 EXPNO 50  
 PROCNO 1

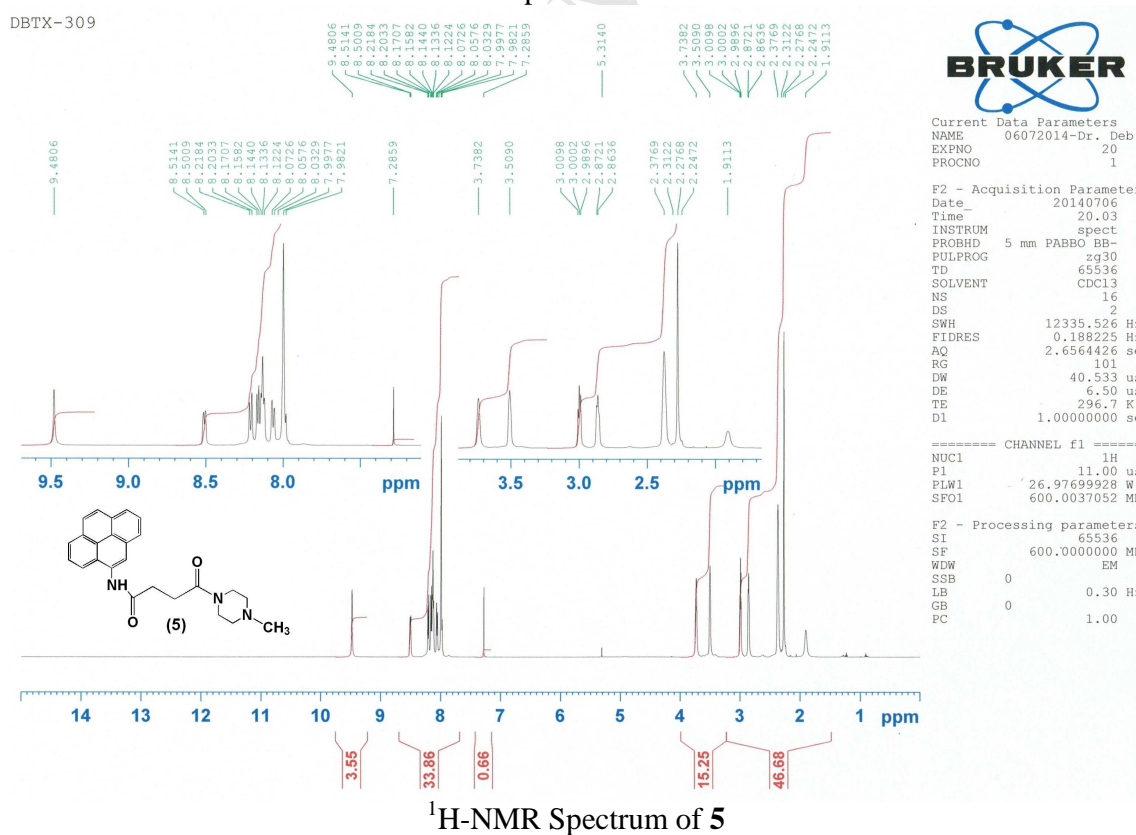
F2 - Acquisition Parameters  
 Date\_ 20120617  
 Time 19.40  
 INSTRUM spect  
 PROBHD 5 mm PABBO BB-  
 PULPROG zg30  
 TD 65536  
 SOLVENT CDCl3  
 NS 16  
 DS 2  
 SWH 12335.526 Hz  
 FIDRES 0.188225 Hz  
 AQ 2.6564426 sec  
 RG 101  
 DW 40.533 usec  
 DE 6.50 usec  
 TE 298.2 K  
 D1 1.00000000 sec

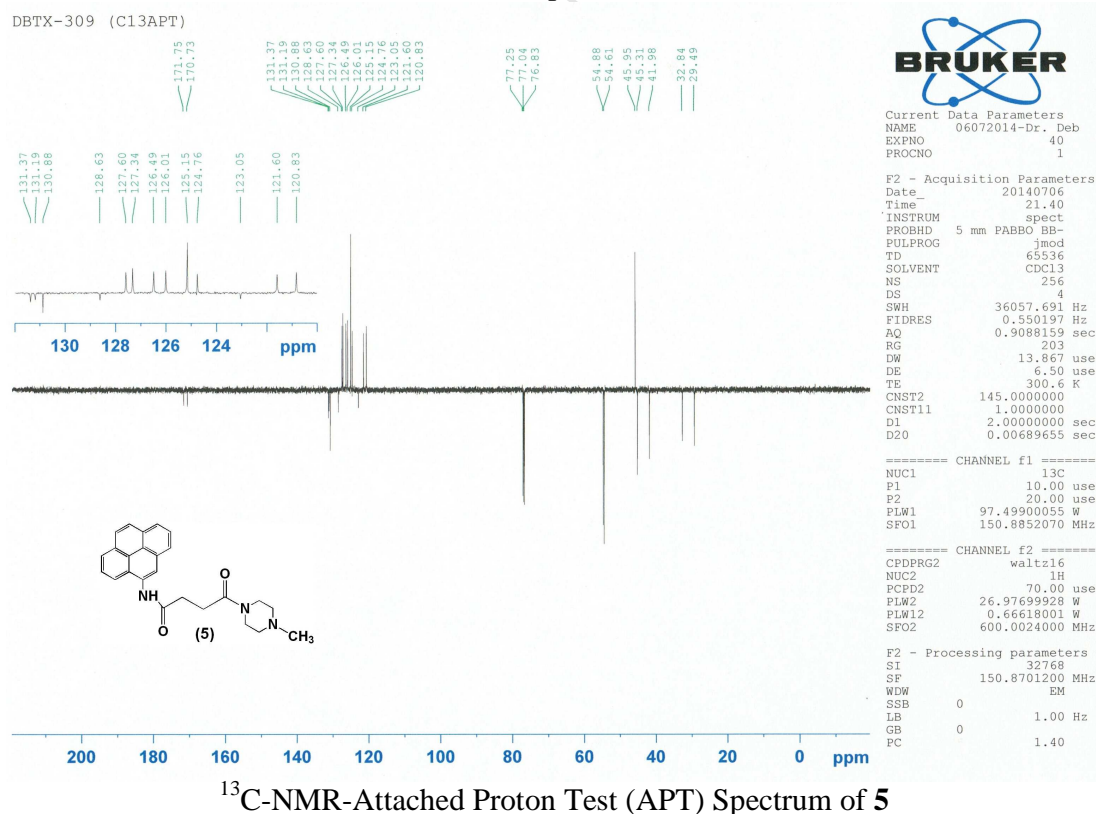
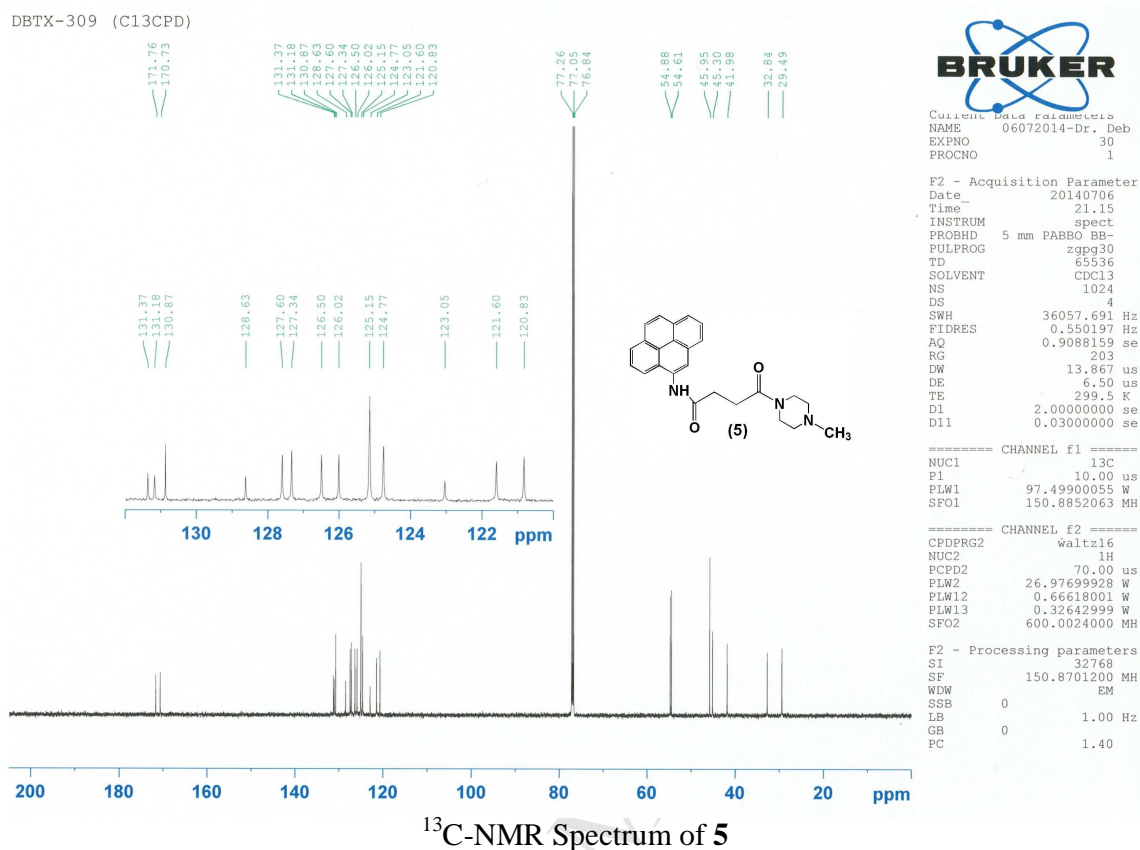
===== CHANNEL f1 =====  
 NUC1 1H  
 P1 11.00 usec  
 PLM1 26.97699928 W  
 SF01 600.0037052 MHz  
 F2 - Processing parameters  
 SI 65536  
 SF 600.0000648 MHz  
 WW EM  
 SSB 0  
 LB 0.30 Hz  
 GB 0  
 PC 1.00

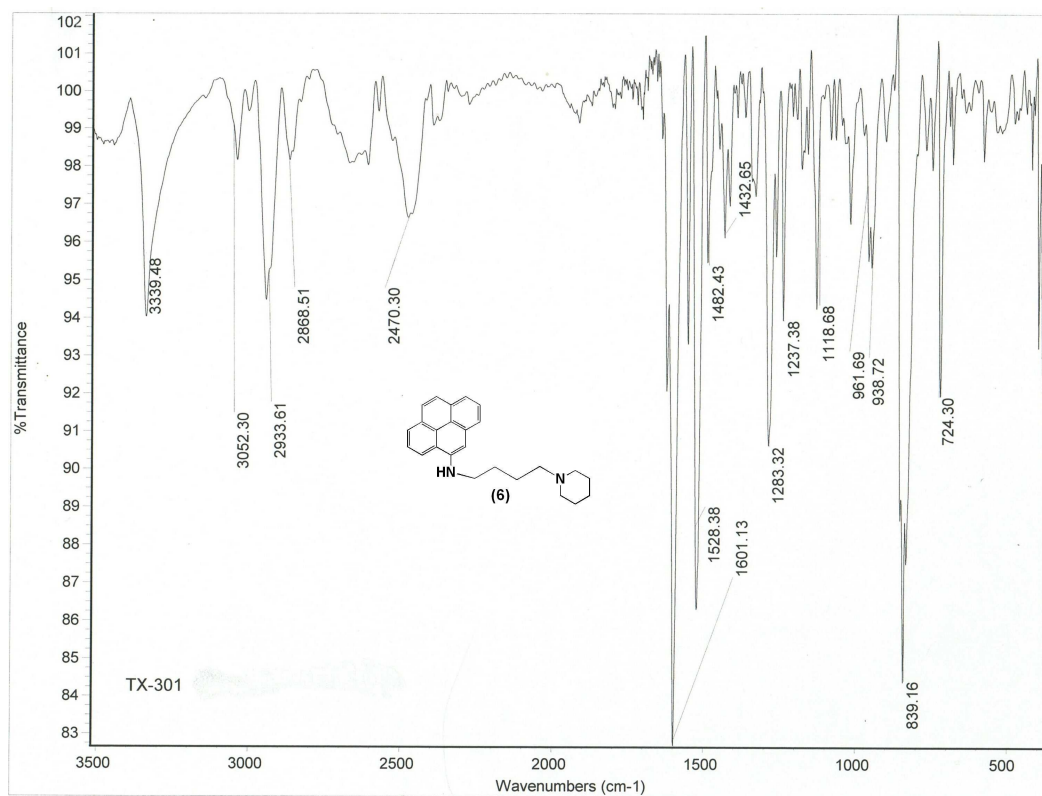




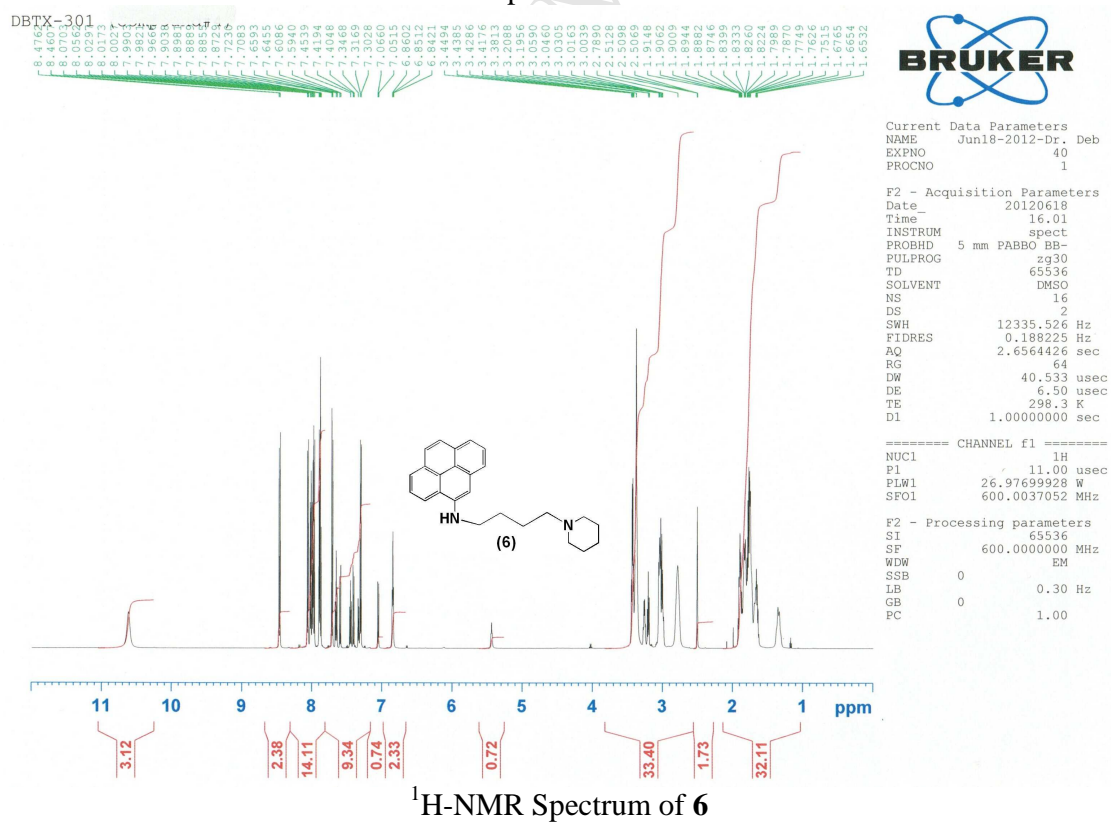
IR Spectrum of 5

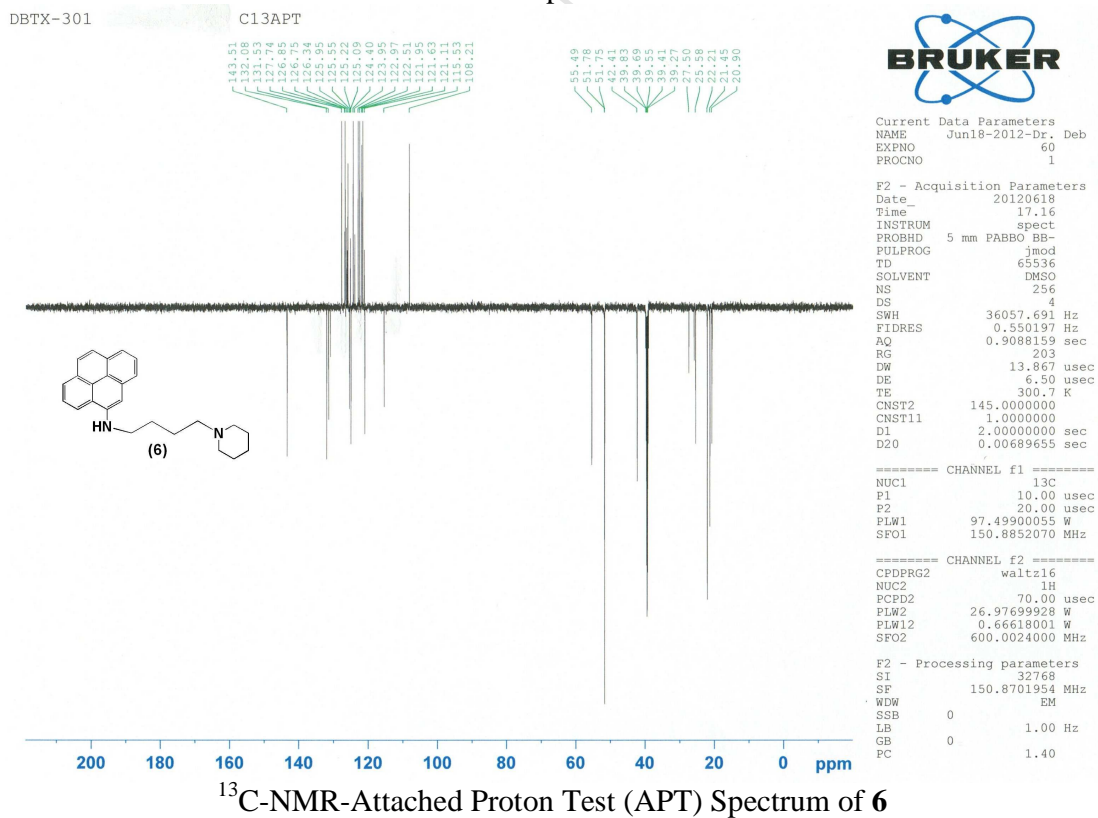
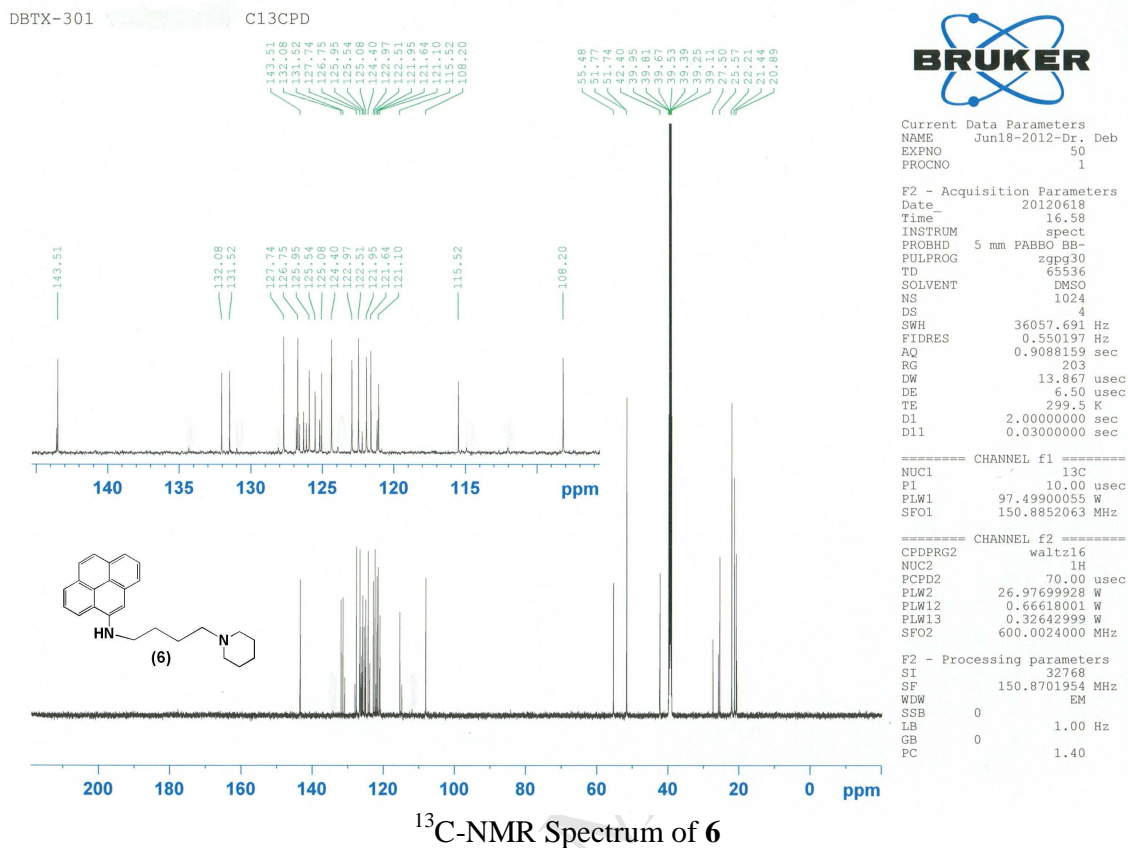
 $^1\text{H-NMR}$  Spectrum of 5

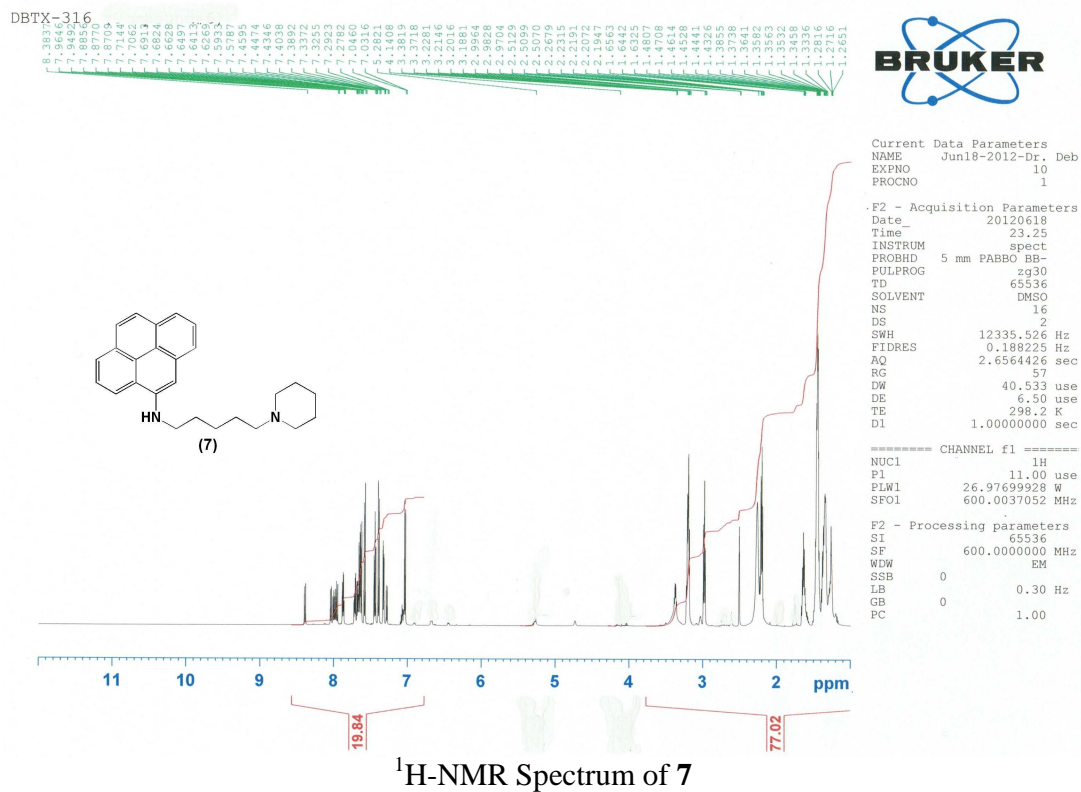
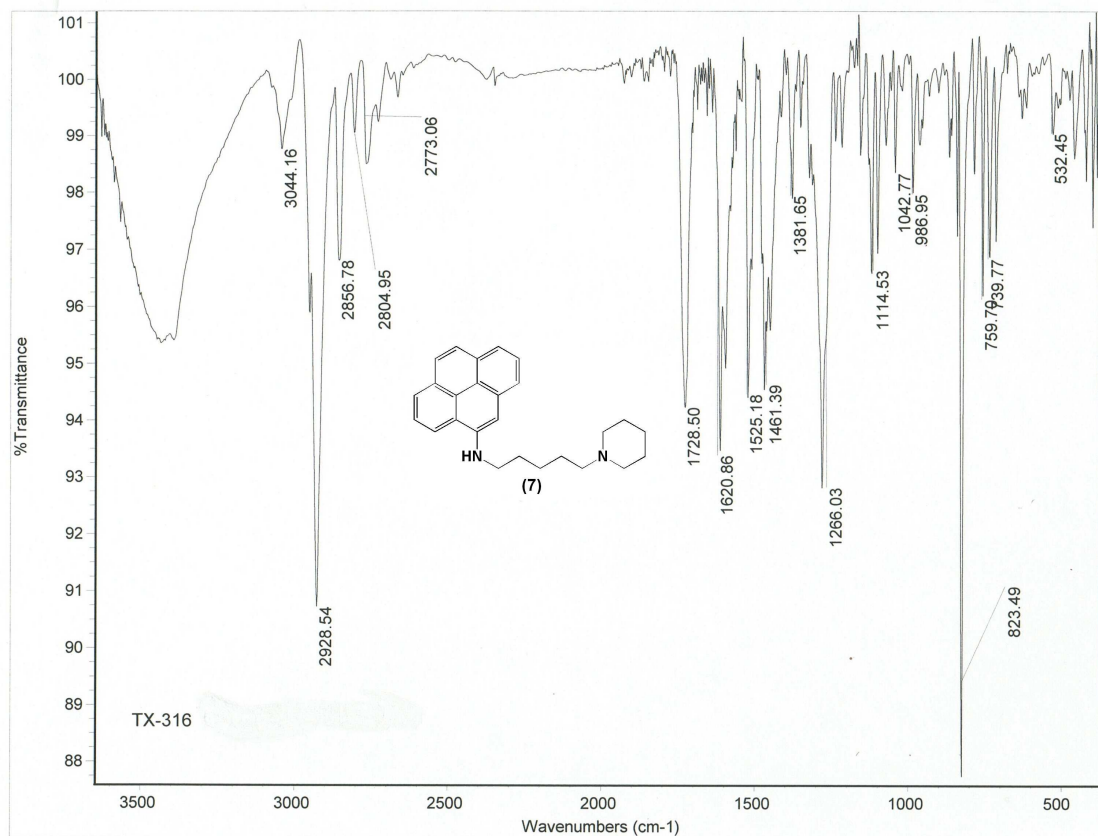


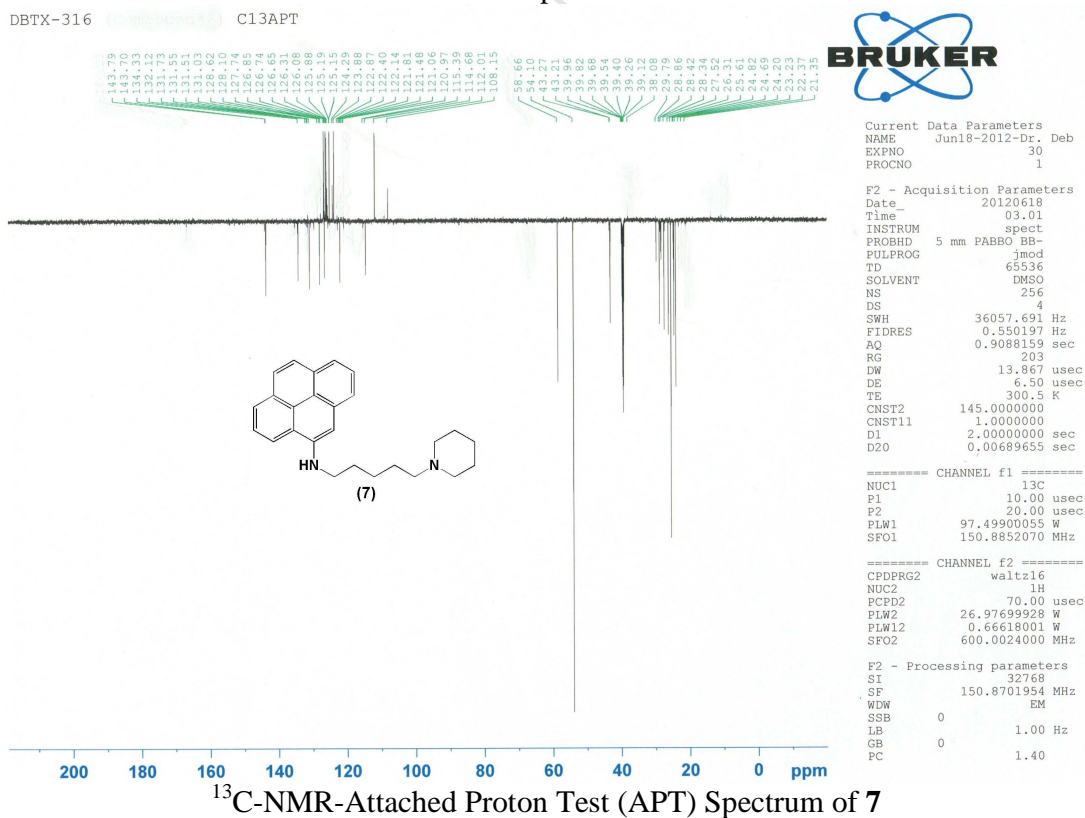
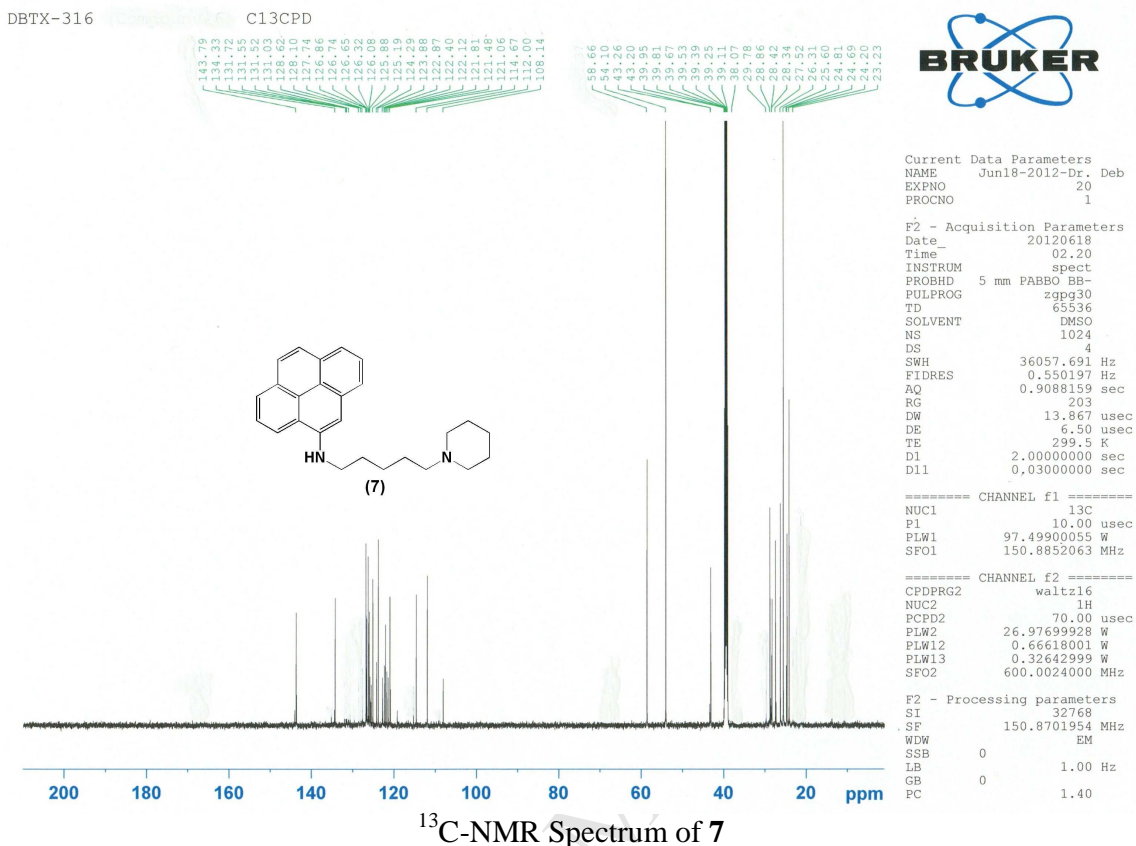


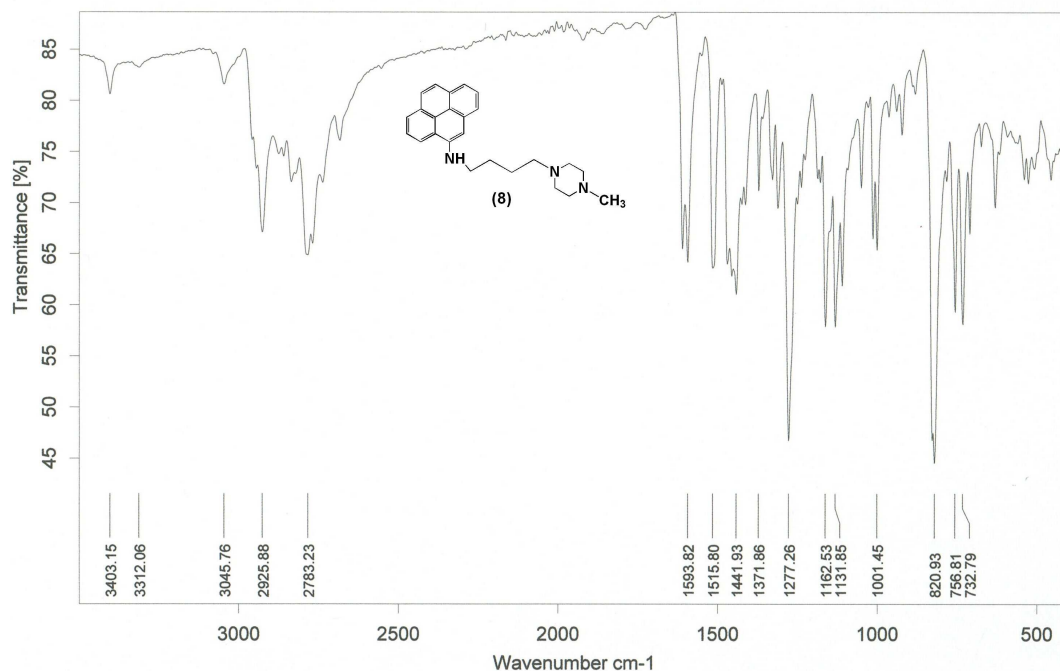
IR Spectrum of 6

<sup>1</sup>H-NMR Spectrum of 6









C:\OPUS\_7.0.129\IBTX-310\IBTX-310.0

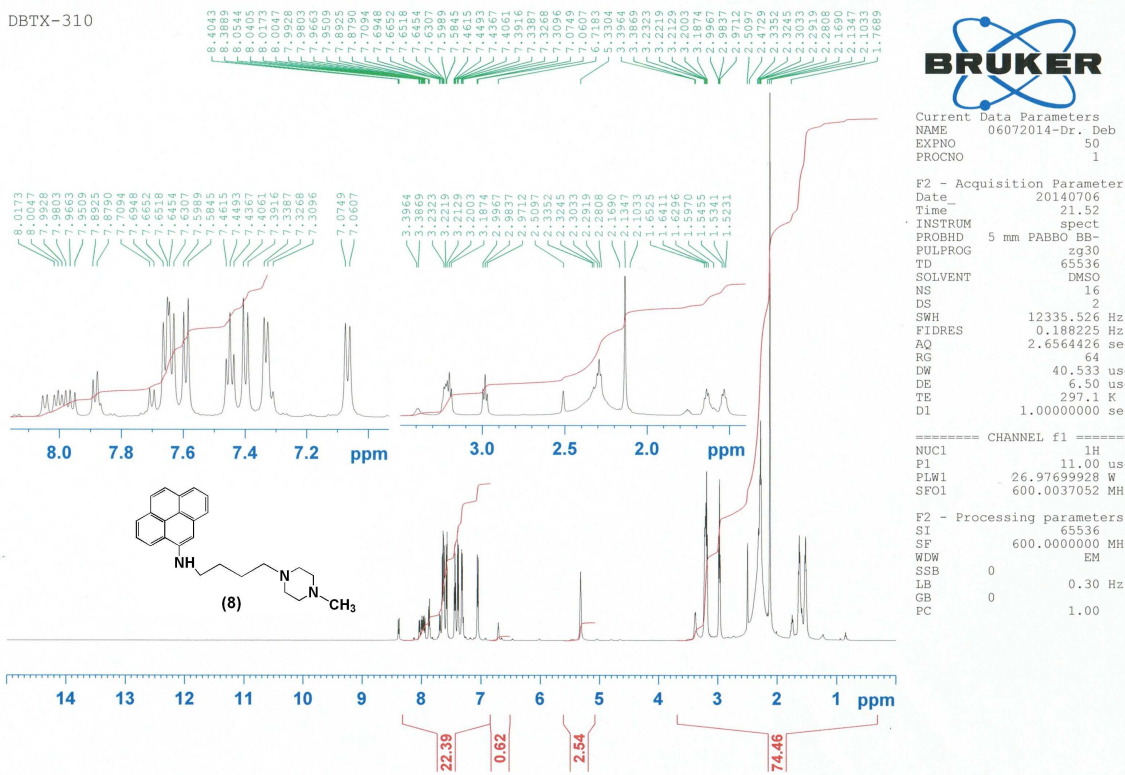
DBTX-310

Instrument type and / or accessory

09/08/2013

## IR Spectrum of 8

DBTX-310

<sup>1</sup>H-NMR Spectrum of 8

DBTX-310 (C13CPD)

